

# Airborne flux measurements of biogenic isoprene over California

P. K. Misztal<sup>1,2</sup>, T. Karl<sup>2,3</sup>, R. Weber<sup>1</sup>, H. H. Jonsson<sup>4</sup>, A. B. Guenther<sup>2,5</sup>, and A. H. Goldstein<sup>1</sup>

[1]{University of California at Berkeley, Berkeley, California, USA}

[2]{National Center for Atmospheric Research, Boulder, Colorado, USA}

[3]{now at: Institute for Meteorology and Geophysics, University of Innsbruck, Innsbruck, Austria}

[4]{Center for Interdisciplinary Remotely-Piloted Aircraft Studies, Monterey, CA, USA}

[5]{now at: Atmospheric Sciences and Global Change Division, Pacific Northwest National Laboratory, Richland, WA, USA}

Correspondence to: P. K. Misztal (pkm@berkeley.edu)

## Abstract

Biogenic isoprene fluxes were measured onboard the CIRPAS Twin Otter aircraft as part of the California Airborne Biogenic volatile organic compound (BVOC) Emission Research in Natural Ecosystem Transects (CABERNET) campaign during June 2011. The airborne virtual disjunct eddy covariance (AvDEC) approach used measurements from a Proton Transfer Reaction Mass Spectrometer (PTR-MS) and a wind radome probe to directly determine fluxes of isoprene over 7,400 km of flight paths focusing on areas of California predicted to have the largest emissions. The Fast Fourier Transform (FFT) approach was used to calculate fluxes of isoprene over long transects of more than 15 km, most commonly between 50 and 150 km. The Continuous Wavelet Transformation (CWT) approach was used over the same transects to also calculate “instantaneous” isoprene fluxes with localization of both frequency and time independent of non-stationarities. Fluxes were generally measured by flying consistently at 400 m  $\pm$ 50 m (a.g.l.) altitude, and extrapolated to the surface according to the determined flux divergence determined in the “racetrack” stacked profiles. The wavelet-derived surface fluxes of isoprene averaged to 2 km spatial resolution showed

1 good correspondence to Basal Emission Factor (BEF) landcover datasets used to drive BVOC  
2 emission models. The surface flux of isoprene was close to zero over Central Valley crops  
3 and desert shrublands, but was very high (up to  $15 \text{ mg m}^{-2} \text{ h}^{-1}$ ) above oak woodlands, with  
4 clear dependence of emissions on temperature and oak density. Isoprene concentrations of up  
5 to 8 ppb were observed at aircraft height on the hottest days and over the dominant source  
6 regions.

7 Even though the isoprene emissions from agricultural crop regions, shrublands, and  
8 coniferous forests were extremely low, observations at the Walnut Grove Tower south of  
9 Sacramento demonstrate that isoprene oxidation products from the high emitting regions in  
10 the surrounding oak woodlands accumulate at night in the residual layer above the valley and  
11 mix down into the valley in the morning. Thus, the isoprene emissions surrounding the valley  
12 have relevance for the regional photochemistry that is not immediately apparent solely from  
13 the direct emission flux distribution.

14 This paper reports the first regional observations of fluxes from specific sources by eddy  
15 covariance from an aircraft which can finally constrain statewide isoprene emission  
16 inventories used for ozone simulations by state agencies. While previously there was no  
17 available means to constrain the biogenic models, our results provide a good understanding of  
18 what the major sources of isoprene are in California, their magnitude, and how they are  
19 distributed.

20 This dataset on isoprene fluxes will be particularly useful for evaluating potential model  
21 alternatives which will be dealt with in a separate paper to assess isoprene emission models  
22 and their driving variable datasets.

23

## 24 **1 Introduction**

25 Isoprene is the dominant Volatile Organic Compound (VOC) playing important roles in  
26 atmospheric chemistry such as fueling tropospheric ozone production, forming secondary  
27 organic aerosols, and acting as important radical sinks in regions near sources. The global  
28 annual source strength of gas-phase biogenic volatile organic compounds (BVOC) is around  
29  $1 \text{ Pg}$  ( $10^{15} \text{ g}$ ) (Guenther et al., 2012). One half of these mass emissions (500 Tg) is constituted  
30 by a single highly reactive hemiterpene, isoprene (2-methyl-1,3-butadiene). The other half is  
31 represented by hundreds to thousands of compounds which span the atmospheric lifetime

1 ranges from a few seconds (e.g. sesquiterpenes) to months (e.g. benzene), and are actively  
2 exchanged in both directions (emission and deposition) between the biosphere and  
3 atmosphere (Park et al., 2013). Currently, BVOC measurements (mostly of emission) have  
4 been reported at ecosystem scales primarily from fixed tower sites which offer very good  
5 temporal resolution, but lack spatial resolution across the broader landscape that is critical for  
6 understanding regional photochemistry.

7 Since the discovery of substantial isoprene emissions from forested regions (Rasmussen,  
8 1970), and subsequent progress in understanding isoprene biochemistry (Loreto and Sharkey,  
9 1990), much research has been conducted to understand the emissions of isoprene and the  
10 factors that drive them at the leaf level, including in California (Arey et al., 1991; Arey et al.,  
11 1995; Baker et al., 1999; Karlik and Winer, 2001; Kurpius and Goldstein, 2003; Goldstein  
12 and Schade, 2000; Schade et al., 1999; Schade et al., 2000; Schade and Goldstein, 2001;  
13 Winer et al., 1992). This work has led to BVOC emission models such as Biogenic Emission  
14 Inventory System (BEIS) (Pierce et al., 1998), Model of Emissions of Gases and Aerosols  
15 from Nature (MEGAN) (Guenther et al., 2012) and Biogenic Emission Inventory Geographic  
16 Information System (BEIGIS) (Scott and Benjamin, 2003) that are driven by information  
17 about weather conditions, plant distributions, leaf area, and the temperature and light  
18 response of isoprene emissions from plants. There have been isoprene flux measurements at  
19 the canopy scale in a variety of locations worldwide: Northwestern U.S. oak savanna (Lamb  
20 et al., 1986), Northeastern US mixed forest (Goldstein et al., 1998), North Central US mixed  
21 forest (Westberg et al., 2001; Apel et al., 2002), Amazonian tropical forests (Rinne et al.,  
22 2002; Kuhn et al., 2002), Central Africa rainforest (Serca et al., 2001), Borneo rainforest  
23 (Langford et al., 2010), etc. However, in California, no ecosystem scale fluxes have ever been  
24 reported for an oak dominated ecosystem that could be used to verify the modeled statewide  
25 isoprene emission inventory.

26 A California BVOC model called BEIGIS (Scott and Benjamin, 2003) predicts significant  
27 emissions of isoprene from oak woodlands distributed throughout the foothills of the Coast  
28 Range and the Sierra Nevada mountains (Figure 1a). However, with the exception of a single  
29 site in a pine plantation (Schade et al., 1999; Schade et al., 2000; Goldstein and Schade,  
30 2000; Schade and Goldstein, 2001), and measurements in a few crops (Karl et al., 2008;  
31 Fares et al., 2011; Fares et al., 2012; Park et al., 2013), there have been no measurements of  
32 BVOC fluxes from California landscapes at a larger spatial scale than individual leaves and

1 branches. The goal of the CABERNET project was to measure the distribution of isoprene  
2 flux across the oak woodland areas of California in order to test and improve the landscape-  
3 scale emission models that are used for regional air quality assessments. The motivation for  
4 conducting this regional flux study in California was driven by: 1) the need for spatially  
5 resolved data on BVOC emissions from oak woodlands which have a large impact on  
6 regional ozone concentrations, and 2) our lack of information on how BVOC emissions  
7 respond to variations in landcover (plant functional type distributions, LAI, etc).

8 California is a region where these observations are particularly needed because of its varied  
9 landscape, with BVOC emissions from biogenic areas dominated by Oaks (~7% of land  
10 area), and with anthropogenic VOC emissions from the activity of ~35 million people living  
11 in the state. Furthermore, the accuracy of isoprene emission estimates is important for  
12 regional simulations of ozone production.

13 Airborne Eddy Covariance (AEC) is an established technique which has been used  
14 extensively in the last several decades to measure fluxes (e.g. of energy, ozone, carbon  
15 dioxide, etc.) directly using an aircraft (e.g. Lenschow et al., 1981; Desjardins et al., 1992;  
16 Pattey et al., 2002; Metzger et al., 2013). The first successful implementation of AEC for  
17 VOC was by Karl et al. (2009) over Mexico using a C130 aircraft.

18 We begin this paper (Sect. 2) by describing the methodology used and the context of the  
19 CABERNET airborne campaign including the study region, climatology, flight-track  
20 planning, aircraft, instrumentation, and the airborne flux methodologies. We then present  
21 results and discussion (Sect. 3) of the isoprene concentration and flux measurements focused  
22 on transects over areas expected to dominate BVOC emissions in California. Stacked  
23 “racetrack” profiles which were used for testing the flux methodology and derivation of flux  
24 divergence terms were recently described in a separate paper (Karl et al., 2013) where we  
25 demonstrated that our PTR-MS configuration in CABERNET was appropriate for measuring  
26 isoprene fluxes. We quantify and discuss the significance of isoprene emissions from the  
27 extensive oak woodlands surrounding the California Central Valley, in which previous  
28 studies considering only concentration measurements, and without an accurate understanding  
29 of isoprene loss rates and regional dynamics, may have underplayed the role of isoprene for  
30 photochemistry in the Valley. Based on simultaneous measurements from a tall tower south  
31 of Sacramento, we demonstrate the abundance of isoprene oxidation products is significant

1 regionally even when the abundance of primary isoprene is low. Finally, we report the first  
2 observed regional spatial distribution of isoprene airborne fluxes and emission factors and  
3 demonstrate that they match well the emission factors from landcovers estimated using a  
4 California Air Resources Board implementation of the MEGAN model. The comparison of  
5 observed fluxes with emissions models will be more thoroughly explored in a separate paper  
6 focused on improving landcover databases and accuracy of isoprene inventories in California  
7 (Misztal et al., 2014).

8

## 9 **2 Methodology**

### 10 **2.1 Study region**

11 Oaks are the main source of isoprene in California and they grow dominantly in certain  
12 elevations (400-800 m) along the foothills encompassing the Central Valley and along the  
13 Coastal Range Mountains. These specific locations, relatively constant elevations, and high  
14 emission rates make oaks an ideal subject for flux observations from aircraft. Using the  
15 USGS National Gap Analysis Program (GAP) landcover database, we planned our survey  
16 flights (to infer surface fluxes from flux measurements over long transects at constant  
17 altitude) and racetrack flights at several levels (vertical profiles to characterize flux  
18 divergence) over more or less homogeneous oak woodlands consisting of the Blue Oak  
19 (*Quercus douglasii*) Woodlands (BOW), Valley Oak (*Q. lobata*) Woodlands (VOW) and  
20 Coastal Oak (*Q. agrifolia*) Woodlands (COW). The total percentage of the sum of their  
21 primary, secondary and tertiary levels was used to map out the most homogeneous areas  
22 where oaks are the only or the dominating tree species (see Sect. 2.3 on flight track planning).  
23 Despite this biological homogeneity the oaks have highly irregular distribution patterns  
24 characterized by varying spatial densities. Supplementary Fig. S1 shows a typical oak  
25 ecosystem as seen from the Twin Otter flying over Tonzi Ranch tower, where ground flux  
26 measurements of isoprene were simultaneously performed for comparison with the aircraft  
27 observations (see Sect. 3.2.2). Apart from relatively homogeneous (in terms of the species)  
28 oak woodlands mostly in the foothill bands, further away there are transition areas with  
29 coniferous regions where, according to the GAP database, the oaks grade in to Blue Oak –  
30 Ponderosa Pine (BOP) habitats and/or Montane Hardwood-Conifer (MHC), and/or Montane  
31 Hardwood (MHW). These areas are represented in Figure 1b.

## 1    **2.2    Climatology during field campaign**

2    Environmental context is important to take into account when analyzing measured isoprene  
3    fluxes because the history of temperature and photosynthetically active radiation (PAR) is the  
4    main driver of potential vegetative emissions (Sharkey et al., 1999; Fuentes and Wang,  
5    1999), and seasonal variability in climate is known to affect gross ecosystem production in  
6    this region (Goldstein et al., 2000). The climatological conditions in California in June 2011  
7    were relatively colder than in June of the previous year. The preceding month and the first  
8    week of June 2011 were particularly cold followed by gradual increase in the temperature  
9    throughout the campaign with particularly hot sunny weather on the final flight of the  
10    campaign. Along with the warming, the environment was becoming dryer.

## 11   **2.3    Flight track planning**

12   The CABERNET airborne campaign took place in June 2011. The paths of the research  
13   survey flights and “racetrack” gradient flights are portrayed over the BEIGIS isoprene  
14   emission factor map (Figure 1a) and California map of oak woodland distribution (Figure  
15   1b). Weather forecasting was used to ensure that all the flights were conducted on cloudless  
16   days, and where possible for the mean wind direction to be perpendicular to the flight paths.  
17   A test flight on June 1<sup>st</sup> was performed over the ocean to calibrate the sensors using pitch and  
18   yaw maneuvers, according to Lenschow (1986). These were used for dynamic upwash  
19   correction and to test the accuracy of coefficients for wind vector transformations to ensure  
20   the vertical wind speed is not affected by aircraft motion. More detailed information on these  
21   maneuvers made during CABERNET can be found in Karl et al. (2013).

22   The true air speed (TAS) was kept as constant as possible on all the flights. For the entire  
23   campaign the TAS ranged from around 52 to 67 m/s with an average of 58 m/s, and a  
24   standard deviation of 2.3 m/s. The measured air temperature at aircraft altitude ranged from  
25   19.4 to 25.9 °C (mean: 22.5 °C, s.d.: 1.28 °C) while the temperature at 2 m above the surface  
26   (WRF model) was wider in range (from 10.9 to 34.8 °C) and higher by 3.6 °C average  
27   temperature.

28   The available forty hours of flight time was divided into eight research flights (RF) which  
29   were carried out for approximately 4-5 hours each during the mid-day.

1 Further information specific to each research flight (RF) is summarized in Table 1 and  
2 described in Supplementary Information.

3

#### 4 **2.4 Aircraft**

5 A two-engine UV-18A Twin Otter (the military version of model Series 300) research  
6 aircraft was operated by the Center for Interdisciplinary Remote Piloted Aircraft Study  
7 (CIRPAS) of the Naval Postgraduate School out of the airport located in Marina, CA near  
8 Monterey, CA. The aircraft is equipped with micrometeorological sensors and is capable of  
9 eddy flux measurements (Karl et al., 2013). Air was drawn from a 3-inch (76 mm) isokinetic  
10 pipe inlet extending above the nose of the plane, resulting in a flow speed inside the tube of  
11 about 10% of the aircraft speed ( $\sim 60 \text{ m s}^{-1}$ ). The vertical wind speed in the airplane  
12 coordinate system was measured by a five-hole radome probe with  $33^\circ$  half-angles at the nose  
13 of the aircraft. The vertical wind speed with respect to the earth is obtained from this  
14 measured vertical wind speed corrected for airplane motions measured by an inertial  
15 reference unit. The measured vertical wind speed is affected by the aircraft movement and  
16 flow distortion at the nose, but this affect can be minimized by applying corrections based on  
17 “Lenschow maneuvers” (Lenschow, 1986). More detailed descriptions of this particular  
18 aircraft can be found elsewhere (Hegg et al., 2005; Reid et al., 2001).

19 The aircraft payload allowed for appropriate instrumentation and between 1 and 3 research  
20 crew on board. The list of instrumentation included: 1) NCAR’s airborne PTR–MS for VOC  
21 fluxes (Karl et al., 2009); 2) NCAR’s custom-built adsorbent-cartridge automatic sampler for  
22 GC-MS VOC speciation and validation of contributions to  $m/z$  measured by the PTR-MS; 3)  
23 a Picarro (1301-m) 2 Hz methane/CO<sub>2</sub> analyzer; 4) a slow ozone analyzer (2B Tech) and dry  
24 chemo-luminescent fast-ozone sensor (NOAA); and 5) a water-based Condensation Particle  
25 Counter (CPC, TSI Inc.).

26 The VOC cartridge sampler containing 8 adsorbent tubes was manually activated during the  
27 flight and was recorded by a datalogger analog input to mark the timing of each sample,  
28 which was drawn automatically through the cartridge for 8 min at a constant flow of 335  
29 standard cubic centimeters per minute (sccm). In addition, one tube served as a blank for each

1 flight and one tube was kept open inside the cabin for passive absorption of VOCs present in  
2 the cabin air to help in the identification of potential tube leaks.

### 3 **2.5 Proton Transfer Reaction Mass Spectrometry (PTR-MS)**

4 The Proton Transfer Reaction Mass Spectrometer (PTR-MS) can measure concentrations of  
5 VOC in a high frequency (10 Hz) virtual disjunct mode (Karl et al., 2002). Unlike a disjunct  
6 sampler which rapidly grabs a sample periodically, a PTR-MS instrument can be regarded as  
7 a virtual disjunct sampler where the ambient air is sampled continuously but  $m/z$  are analyzed  
8 sequentially by the quadrupole detector, creating a disjunct dataset with high frequency data  
9 (e.g. 10 Hz) separated by a relatively longer gap (e.g. 0.5 s). Thus, the 10-Hz disjunct  
10 sampling corresponded to 0.1-s dwell time and approximately 2 samples/s.

11 The instrument deployed in CABERNET was NCAR's high sensitivity PTR-MS (Karl et al.,  
12 2009). Its internal vacuum inlet system was specifically redesigned to enable stable operation  
13 across a wide range of altitudes and to ensure internal lag-time of less than 100 ms. The  
14 instrument operation and routine were kept consistently constant for each flight. Current FAA  
15 regulations do not allow for the instrumentation to be running overnight, requiring specific  
16 steps to achieve stable instrument operation quickly after an instrument start-up. A flight-  
17 optimized vacuum system and internal capillary components result in fast transfer time from  
18 the inlet to the drift tube and independence of ambient pressure variations on the drift-tube  
19 pressure at high altitudes. The valves between the water reservoir and the ion source reduce  
20 the time to achieve ion source stability and low oxygen ion levels in the drift tube.  
21 Approximately three hours before the take-off the instrument was powered up, and  
22 approximately 1 hour before the take-off, if the  $O_2^+$  signal went below 6% of the primary  
23 ions, a secondary electron multiplier (SEM) and ion source check with optimization was  
24 followed by a dynamic calibration using two VOC standards (Apel-Riemer), one high  
25 concentration (available during pre-flight) containing low-fragmenting compounds for daily  
26 sensitivity curves (i.e. benzene (1.11 ppm), toluene (1.07 ppm), xylenes (4.22 ppm),  
27 trimethylbenzene (1.94 ppm), dichlorobenzene (2.61 ppm), and trichlorobenzene (1.14 ppm))  
28 diluted with VOC-free air and another low-concentration standard containing isoprene (10.0  
29 ppb) (also available in-flight) which was also used as a back-flushing gas during the take-offs  
30 and touch-downs to prevent the exhaust plumes from contaminating the inlet. Zeros were  
31 measured using three different sources: Pt-catalyzed ambient air; ultra-pure compressed air



1 (Air Liquide); ambient air at the top of the saw-tooth sounding well above the PBL height.  
2 The calibrated normalized sensitivities for calibrated VOCs experienced day-to-day  
3 variabilities of less than 30%. The average sensitivity for isoprene was 15.1 normalized  
4 counts per second per ppbv (ncps ppbv<sup>-1</sup>) as a sum of *m/z* 69 (13.4 ncps ppbv<sup>-1</sup>) and *m/z* 41  
5 (2.2 ncps ppbv<sup>-1</sup>). The *m/z* 41 ion was used to assess the stability of isoprene fragmentation  
6 but only *m/z* 69 was used in the calculation of concentrations. These high sensitivities  
7 ensured low detection limits (e.g. <10 pptv for isoprene at 1-km averaging (~17 s)). The  
8 primary ion count rates monitored at *m/z* 21 were around 2.0·10<sup>7</sup> counts per second (cps)  
9 (±20%) so the absolute sensitivities were approximately 20 times higher than the normalized  
10 sensitivities (i.e. ~300 cps ppbv<sup>-1</sup> for isoprene). The sensitivities for compounds not present in  
11 the standard were approximated for each day from combining sensitivity curves of the daily  
12 calibrations with sensitivity curves from post-campaign calibrations using several different  
13 standards at a range of humidities. The accuracy of sensitivities was estimated at ±10% for  
14 direct calibration (5% standard certification + 5% from dilution) and ±30% for the approach  
15 combining post-campaign calibrations. The settings, sensitivities and further methodological  
16 remarks are included in Supplementary Table S1.

## 17 **2.6 Airborne eddy covariance (AEC)**

18 The preferred micrometeorological method for measuring trace gas fluxes in the turbulent  
19 boundary layer is eddy covariance (EC). This approach is a direct measurement of the  
20 fluctuating vertical wind velocity and trace gas concentration. The flux is determined from  
21 the mean covariance between vertical wind velocity (*w*) and concentration (*c*) fluctuations  
22 and can be expressed as

$$23 \quad F = \overline{w'c'} \quad (1)$$

24  
25 where *w'* is the difference between the instantaneous and mean vertical wind speed and *c'* is  
26 the difference between the instantaneous and mean trace gas concentration. Here we use  $\overline{w'c'}$   
27 to represent the time average of the product of these two variables. The major components of  
28 an EC flux system are: 1) a system that measures vertical wind speed with a fast (typically  
29 <100 ms) response time; 2) an instrument that measures the targeted atmospheric constituent

1 with a fast response time; and 3) a system to receive and store the data (e.g, datalogger or  
2 computer). Instruments with slower ( $> 100$  ms) response times can be used to measure the  
3 flux associated with lower frequencies but may underestimate the total flux depending on the  
4 frequency of the transporting eddies. In some cases this may result in an acceptable error  
5 while in other cases an attempt can be made to account for the loss of flux due to inadequate  
6 sensor response (Moore, 1986; Rowe et al., 2011). One way for estimating high frequency  
7 correction involves using another scalar that is measured with a fast response sensor and then  
8 estimating the reduction in flux that results if a digital filter is used to simulate response time  
9 of the slower instrument.

10 EC is used extensively to measure sensible and latent heat fluxes, and has recently been used  
11 for networks dedicated to quantifying carbon dioxide fluxes from various landscapes  
12 (Baldocchi, 2003). Commercial fast response instruments are available for some compounds  
13 (e.g. CO<sub>2</sub>, H<sub>2</sub>O, CH<sub>4</sub>) and others can be constructed for additional chemical species. EC is  
14 generally preferred as the most direct flux measurement method which does not require  
15 parameterizations. Fluxes of VOC with short lifetimes can be estimated from flux divergence  
16 measurements (Lenschow et al., 1980).

17 Wyngaard and Brost (1984) proposed that the surface fluxes could also be estimated from  
18 measurements of vertical concentration profiles in the daytime convective boundary layer  
19 (CBL) that lies above the surface layer and can extend up to several km. This method  
20 assumes that the mean vertical gradient of a conserved species in the CBL is determined by  
21 the depth of the CBL ( $z_i$ ), the convective velocity scale ( $w^*$ ), and the fluxes at the bottom and  
22 the top of the CBL. We used vertical profiles of temperature and humidity measured during  
23 “saw-tooth soundings” (steep climbs through PBL and part of the free troposphere [e.g. up to  
24 3 km] at a constant angle followed by the similarly steep descent) to directly characterize  $z_i$   
25 and measured sensible heat fluxes to quantify  $w^*$ . The CBL gradient-flux technique assumes  
26 that boundary layer mixing is dominated by convective turbulence and that boundary layer  
27 conditions evolve slowly compared to the convective turnover time of about 7 minutes. The  
28 results are not affected by vertically homogeneous horizontal advection or time dependence  
29 in the mean concentration and the method can account for entrainment.

30 A time scale at a fixed point in the PBL can be related to a length scale by multiplying the  
31 time scale by the average wind speed, as long as the “frozen turbulence” hypothesis known as

1 Taylor's hypothesis (e.g. Panofsky and Dutton, 1984) is fulfilled. This hypothesis enables  
2 approximate conversion from temporal to spatial statistics. Since aircraft can fly an order of  
3 magnitude faster than the mean wind, Taylor's hypothesis is more easily fulfilled, so the  
4 length scales can be calculated by multiplying the measured time scale by the true airspeed.

5 Area source emission was measured using the airborne eddy covariance technique. Eddy  
6 covariance was used to directly measure fluxes of predetermined compounds. Because  
7 quadrupole systems analyze mass to charge ratios sequentially, only a small number of  
8 compounds can be selected for inclusion into the flux mode to keep the disjunct gap  
9 relatively small. The number of masses ranged from three to six during eight research flights.  
10 As the project was focused on California vegetation and in particular oak woodlands,  
11 isoprene ( $m/z$  69) was measured on all eight research flights, MVK+MACR ( $m/z$  71) and  
12 methanol ( $m/z$  33) on seven flights. Other VOCs measured on a smaller number of flights  
13 included monoterpenes ( $m/z$  81, 137), MBO ( $m/z$  87), acetaldehyde ( $m/z$  45), benzene ( $m/z$   
14 79), toluene ( $m/z$  93), and C8-aromatics ( $m/z$  107). In this manuscript, we focus solely on the  
15 isoprene concentration and flux observations. Spatially resolved eddy covariance fluxes were  
16 calculated using Wavelet Analysis (Mauder et al., 2007) along flight tracks through the  
17 convective layer. Since the majority of flights were conducted in the lower part of the mixed  
18 layer and the upper part of the surface layer (typically 100-200 m deep based on 10% of the  
19 measured PBL depth), we estimate the horizontal spatial resolution based on the blending  
20 height (e.g. Claussen, 1990) using the surface layer scaling and the parameterizations for the  
21 mixed layer scaling (Karl et al., 2013).

### 22 2.6.1 Airborne virtual Disjunct Eddy Covariance (AvDEC)

23 The difference between virtual and conventional disjunct eddy covariance is that sampling  
24 flow is continuous but the dataset becomes disjunct because the quadrupole detector cycles  
25 through the  $m/z$  sequentially, producing regular gaps between high-frequency data points. For  
26 the small number of  $m/z$  scanned by the PTR-MS detector, AvDEC measurements are nearly  
27 equivalent to continuous AEC. In order to minimize the disjunct error the number of samples  
28 collected per integral scale should significantly exceed 1 and the effective duration of the  
29 sample period should be maximized. This can be achieved by limiting the number of  $m/z$  in  
30 the duty cycle and keeping the integration time long. We kept the number of VOC-related  $m/z$   
31 between 3 and 6 at 0.1 s dwell time. In addition, on each flight, we monitored three control

1 masses: hydronium ions ( $m/z$  21), oxygen ions ( $m/z$  32), and water vapor ( $m/z$  37) at 0.1, 0.05,  
2 and 0.05 s, respectively, so the total duty-cycle length varied from 0.5 to 0.8 s between  
3 different flights which resulted in a sampling rate of 1.25 to 2 samples/s.

#### 4 2.6.2 Fast Fourier Transform (FFT)

5 Fast Fourier Transform (FFT) is the conventional method to compute airborne flux. This  
6 method provides a single value for a given segment of flight, which limits the spatial  
7 resolution. The optimal stretch for flux calculation would be a sufficiently long pass to  
8 capture the optimal range of frequency distribution, but not so long that the turbulent  
9 structures are affected by diurnal effects. Therefore, resolution finer than 10 km would be  
10 challenging and uncertain using the FFT approach. Another challenge in this method is that it  
11 is affected by non-stationarities (e.g. related to heterogeneities). However, as an independent  
12 method it can be very useful for comparison with fluxes obtained from wavelet analysis (see  
13 Sect. 2.6.3).

#### 14 2.6.3 Continuous Wavelet Transform (CWT)

15 Wavelet analysis, originally demonstrated to work with seismological data, has recently  
16 become increasingly popular in environmental and biological applications. Examples can be  
17 found in the analysis of the turbulent structures (Thomas and Foken, 2005; Mauder et al.,  
18 2007; Steiner et al., 2011; Metzger et al., 2013), and analysis of environmental processes at  
19 multiple scales (Stoy et al., 2009; Vargas et al., 2010).

20 The mathematic principle for the one-dimensional wavelet transform of a given signal  $f(t)$  can  
21 be presented as:

$$22 \quad T_p(a,b) = \int_{-\infty}^{+\infty} f(t) \overline{\Psi_{p,a,b}(t)} dt, \quad (2)$$

23

24 where  $T_p(a,b)$  are wavelet coefficients and  $\Psi_{p,a,b}(t)$  is the wavelet function given by:

$$25 \quad \Psi_{p,a,b} = \frac{1}{a^p} \Psi\left(\frac{t-b}{a}\right), \quad (3)$$

26

1 where  $\Psi((t - b)/a)$  is termed "the mother wavelet", of which shape and locations are  
2 determined by the scale parameter of the wavelet  $a$  and by the translation parameter  $b$ . The  
3 normalization factor  $1/a^p$  preserves the energy of the original mother wavelet (for  $p=1$ ). A  
4 general description of wavelet methodology can be found in Torrence and Compo (1998). We  
5 used the Morlet mother wavelet, but there are different types of mother wavelets which can  
6 be suitable for different applications. For example, the Mexican-Hat mother wavelet works  
7 well with detection of single events, for example in the analysis of coherent structures of  
8 ejections and sweeps from a closed-canopy forest (Steiner et al., 2011). On the other hand,  
9 the complex Morlet function wavelet is suited to analysis of variance spectrum (Thomas and  
10 Foken, 2007). Nordbo and Katul (2013) looked at periodicities of long-term CO<sub>2</sub> fluxes from  
11 soil. They showed that the intrinsic smoothing property of the wavelet produces results that  
12 are more easily interpretable, without the need of excessive manipulation of the original  
13 signal (e.g. averaging, smoothing, and tapering) or without restrictive assumptions (e.g.  
14 periodicity, stationarity).

15 The CWT method has an advantage over FFT in that it does not require homogeneity or  
16 stationarity, and can reconstruct the time domain to provide specific information on where in  
17 space/time and on which frequency the flux occurs. The wavelet flux method allows for the  
18 reconstruction of both the frequency and time domains of the flux within a straight stretch of  
19 the desired length, and therefore can produce "instantaneous" or "discrete" fluxes which can  
20 be directly compared with model estimates. From the pragmatic point of view, calculation of  
21 an entire flight segment (e.g. of 100 km) results in not just a single flux value but delivers  
22 spatially resolved fluxes at discrete intervals sometimes informally referred to as  
23 instantaneous fluxes. Considering the footprint and wavelet scaling parameters, it is possible  
24 for an aircraft flying low at approximately 60 m s<sup>-1</sup> to provide meaningful spatial flux  
25 representation at the 1-2 km resolution needed for investigating landscape heterogeneity in  
26 high resolution biogenic emission models, although in principle even shorter intervals could  
27 also be resolved. However, the segment to average the CWT fluxes needs to be sufficiently  
28 long to capture all the frequency contributions (e.g. of the order of the PBL depth). We  
29 determined that for a sufficiently long stretch (e.g. 20-200 km) it is possible to achieve  
30 statistically significant discrete wavelet fluxes, on the order of hundreds of meters. To  
31 comply with the range of conditions and to ensure statistical significance for the given  
32 surface patchiness, the 2 km flux is not just a single value but it is an aggregate of individual

1 wavelet flux values averaged to 2 km. These 2-km fluxes make it flexible to further average  
2 spatially to reduce random error related to high variability at short time scales (see Sect. 2.7),  
3 before comparing observations with model emissions. An average of the wavelet fluxes can  
4 be compared to the Fourier flux from the same stretch. Given the independent approaches, the  
5 agreement between the methods adds to the confidence of the flux estimates and the ratio can  
6 be used as an additional measure of data quality. Finally the co-spectra from the two methods  
7 can be compared. If no high-frequency attenuation losses exist, the co-spectra should be  
8 similar. The wavelet approach can also be used for the correction of the FFT high-frequency  
9 spectral attenuation if it is related to tubing effects or factors other than the instrument  
10 response (Nordbo and Katul, 2013). More detailed methodology of wavelet analysis used in  
11 this work has been presented by Karl et al. (2013) which was a further development from  
12 Karl et al. (2009).

13

#### 14 2.6.4 Vertical flux

15 Vertical flux divergence of isoprene is expected to be primarily controlled by its relatively  
16 short lifetime and was measured directly using “racetracks” at multiple altitudes (Karl et al.,  
17 2013). It was found to be similarly linear above different oak ecosystems and heterogeneity.  
18 We estimated the contribution of the storage term to the isoprene flux divergence to be of the  
19 order of 2-5%, relatively small compared to the storage term in the temperature budget.  
20 Fluxes were generally measured by flying consistently at 400 m  $\pm$ 50 m (a.g.l.) altitude, which  
21 was chosen so that the resulting blending length and flux footprint match the spatial scale of  
22 surface patchiness (Mahrt, 2000; Raupach and Finnigan, 1995; Wood and Mason, 1991;  
23 Mason, 1988). The flux at the aircraft altitude was typically in the range of 5% to 30%  
24 smaller than the surface flux depending on the ratio of aircraft altitude to PBL height ( $z/z_i$ ),  
25 and the determined flux divergence linear coefficients were assumed to be relatively constant  
26 based on the range of OH concentration estimates for the entire flight track. An alternative  
27 method expected to work with similar accuracy would be to use inverse models (Bange et al.,  
28 2006). The wavelet coefficients were optimized for the CWT analysis to perform well on  
29 stretches between 15 and 200 km with a typical ratio of FFT single flux value to CWT  
30 instantaneous flux average of between 1.0 and 1.3.

## 1 2.6.5 Flux footprints

2 The footprint for each flux point was derived using the Weil and Horst (1992) approach and  
3 depends on the wind speed, relative altitude to the PBL height, and the convective velocity  
4 scale.

5 Here we use scaling developed for the mixed layer according to:

$$6 \quad dx_{0.5} = 0.9 \frac{u \cdot z_m^{2/3} \cdot h^{1/3}}{w^*}, \quad (4)$$

7 where  $dx_{0.5}$  is the half width of the horizontal footprint,  $u$  the horizontal windspeed,  $z_m$  the  
8 height above ground,  $h$  the PBL height and  $w^*$  the convective velocity scale which is derived  
9 from the wavelet heat flux in each transect.

10 The source contribution area can be approximated by projecting an upwind-pointed half  
11 dome with the  $dx_{0.5}$  parameter representing a radius of that half dome (see Supplementary  
12 Fig. S5).

## 13 2.7 Error analysis (quality of fluxes)

14 As with eddy covariance on the ground, AEC fluxes must undergo a rigorous quality  
15 assessment, if not more so. The total uncertainty in reported airborne flux for a typical flight  
16 segment ( $> 20$  km) is the summation of errors from calculation of concentrations (10% for  
17 calibrated compounds [5% standard accuracy+5% dilution system], 30% from relative lab-  
18 based sensitivity-relative transmission approach), survey-flight-specific random (15% for the  
19 typical leg), systematic (1%) errors related to relative altitude within the PBL and to the  
20 aircraft leg, random error related to disjunct measurement (less than 1%), error due to storage  
21 term (2%) and error due to variability in flux divergence coefficients ( $\sim 2\%$ , explained further  
22 below). For reactive tracers which require divergence corrections to yield the surface flux,  
23 uncertainty in PBL estimation (interpolated from saw-tooth soundings) is  $\pm 100$  m which  
24 translates to 10% of up to 30% of the divergence correction, thus  $\sim 3\%$ . We estimate the total  
25 accuracy for the reported surface fluxes averaged for long segments (e.g. 100 km) to be 30%  
26 for calibrated compounds and 50% for other compounds and a typical isoprene flux detection  
27 limit of  $0.01 \text{ mg m}^{-2} \text{ h}^{-1}$ .

1 The vertical flux divergence is dependent on the rate of isoprene oxidation (which depends  
2 mostly on OH concentration during daytime), the time rate of change of isoprene  
3 concentration (relevant also for conserved species), and differential horizontal advection of  
4 isoprene with height (small). Based on directly measured flux divergence in the racetrack  
5 gradient flights (Karl et al., 2013) we showed clear linear dependence of the flux divergence  
6 with a theoretical vertical concentration gradient (e.g.  $1.4 \times 10^{-4}$  ppbv  $m^{-1}$  over a homogenous  
7 oak terrain and an OH concentration of  $6.6 \times 10^6$  molec/ $cm^3$ ). Since the flux divergence for  
8 isoprene was shown to be primarily controlled by OH concentrations (of which we have a  
9 range of estimates), we make an informed assumption here that the divergence coefficients  
10 we used to scale the fluxes to the surface are accurate within a factor of two for the entire  
11 campaign. Thus a change in the flux divergence coefficients by a factor of two could result in  
12 only a ~2% difference to the scaled surface flux for a typical  $z/z_i$  ratio of 0.3 which is minor  
13 relative to other error sources as discussed above. As the correction of the fluxes for flux  
14 divergence was typically less than 20%, the contribution from less accurate divergence  
15 coefficients is assumed to be relatively minor (up to ~2%) for isoprene.

16 The uncertainty of the instantaneous CWT fluxes aggregated to 2-km is dominated by the  
17 random error which must be necessarily larger than that for the average flux for the whole leg  
18 and is related to high temporal and spatial variability (e.g. Mann and Lenschow, 1994). Using  
19 equation 3 from Karl et al. (2013) this error can be of the order of 40-50% but declines with  
20 averaging of the 2-km points and is already below 30% when averaging more than 5 km. For  
21 this reason we have only evaluated fluxes over longer stretches ( $\gg 2$  km). The 2-km  
22 representations can provide more flexibility for averaging, for example, individual points can  
23 be useful for a regression of isoprene flux versus LAI for all of the 2-km data providing  
24 excellent statistics. However, it makes sense to use spatially averaged data (e.g. regional  
25 zones) for comparison with the models. While the footprint averaged data are not shown here,  
26 such data would be additionally associated with the error related to footprint accuracy which  
27 is related to uncertainty in short-term convective scale velocity, PBL height and any  
28 variability in wind speed. Thus, the total uncertainty of the surface fluxes of isoprene is  
29 estimated at approximately 50% for individual 2-km data points, but at 20% for averages  
30 exceeding 10 km.

31 The calibrated concentration data filtered for interferences (e.g. a biomass burning episode;  
32 see supplementary video) were used with corrected vertical wind speed data to derive



1 covariance functions for each eligible stretch. The segments were selected for flux calculation  
2 based on minimal roll angle of the aircraft between turns, and on consistency of altitude,  
3 excluding maneuvers with significant altitude changes such as soundings (see example in  
4 Supplementary Fig. S2). Of segments prescreened for validity, only those with a clear peak in  
5 the covariance function (Figure 2a) within the lag-time window of 5 s were accepted. The  
6 segment data were subsequently examined for similarities in the variances of concentration  
7 and vertical wind speed (Figure 2b) together with the time series of wavelet frequency co-  
8 spectra (Figure 2c) within the cone of influence (COI) which is the region where the end of  
9 the power spectrum may be impacted by edge effects. Rather than excluding the part falling  
10 outside the COI, each of the ends of the time series are padded with zeros and excluded  
11 afterward, so the results are not affected by the COI. By comparing the wavelet co-spectra  
12 with average cross-covariance (Figure 2d) it is possible to determine where in the wavelet  
13 period (inverse of frequency) the flux contribution occurs, enabling for example the  
14 visualization of the updrafts associated with high emissions.

15 Each stretch was finally analyzed for spectral characteristics, independently for the FFT and  
16 CWT methods (see Figure 3). Identical procedures were applied to the fast temperature  
17 sensor for comparison. As the co-spectra and ogives demonstrate, the VOC sampling system  
18 was not limited by high frequency attenuation owing to the short 0.1 s dwell time and small  
19 number of preselected VOCs in the quadrupole mass spectrometer cycle. It was found that  
20 the majority of the flux contribution (~90%) was occurring between between 0.1 and 0.01 Hz  
21 which translates to the spatial scales of 0.6 to 6 km.

22 Additional quality measures were the ratio of the FFT and CWT fluxes (Figure 4, upper  
23 panel), which for isoprene were usually  $1 \pm 15\%$  for survey transect flights. Identical values  
24 from the two methods were not expected as the FFT flux is affected by nonstationarities and  
25 inhomogeneities in contrast to the CWT flux, but the generally good agreement adds  
26 confidence to the results. Occasionally, a ratio higher than 1.15 was seen on short segments,  
27 or over a nonhomogeneous transect, or when the fluxes were close to zero. In sporadic cases  
28 when the fluxes were strongly non-stationary (characterized by the ratio higher than 1.3), the  
29 FFT flux was tagged as rejected and the CWT flux was only accepted if all the other quality  
30 criteria were fulfilled.

1 The generally good quality of fluxes in CABERNET was due to a combination of factors  
2 such as instrument sensitivities, response times, slow aircraft speeds and proximity to the  
3 source by flying at low altitudes (e.g. 400 m) and finally lack of spectral interferences (e.g.  
4 from propellers). Figure 4 (lower panel) shows the application of flux divergence (only  
5 reactive compounds such as isoprene) coefficients from racetrack profiling to derive the  
6 surface fluxes from the aircraft fluxes. In the remainder of the manuscript when discussing  
7 fluxes, we focus exclusively on the CWT fluxes due to the much higher spatial resolution of  
8 the flux and also because of their higher accuracy in cases with inhomogeneity and non-  
9 stationarity.

### 10 2.7.1 Simultaneous ground based measurements

11 Ground based measurements coinciding with aircraft passes in time and space were  
12 performed at two sites: The 525-m tall Hearst-Argyle Tower in Walnut Grove, California  
13 (WGC) located in the San Joaquin Delta region south of Sacramento (38.2636, -121.4899,  
14 elevation 1 m) and the 23-m tall Tonzi Ranch Tower (TRT) (38.4308, -120.9656, elevation  
15 177 m) located in the relatively homogenous oak forest savannah below the Sierra Nevada  
16 foothills to the east of the San Joaquin Delta. Description of these measurements is provided  
17 in Supplementary Information.

18

## 19 3 Results and discussion

### 20 3.1 Observed concentrations of isoprene from PTR-MS

21 The spatial distributions of isoprene concentrations measured on all research flights are  
22 shown in Figure 5.

23 Isoprene concentrations were low, typically less than 50 ppt ( $0.05 \text{ mg m}^{-2} \text{ h}^{-1}$  in fluxes) in the  
24 Central Valley at flight altitude over agricultural terrains and over urban areas but were very  
25 high over the oak woodlands which cover approximately 7% of California, and were the  
26 focus of the CABERNET campaign flight plans. In general, observed isoprene concentrations  
27 over oak woodlands ranged from less than 1 ppb on cool days up to several ppb on warmer  
28 flights. A maximum of 8 ppb was observed on the hottest day. The aircraft also saw marked  
29 increases of isoprene near some highways with eucalyptus trees planted alongside. Although

1 no study of regional scale emissions of VOC in California was previously conducted, the  
2 pattern of concentrations observed during CABERNET is consistent with an expected pattern  
3 based on extrapolation of earlier studies from enclosures of dominant plant species of  
4 California which suggested oaks (mostly blue oaks), and to some degree eucalyptus trees, to  
5 be likely the most important isoprene emitters in California (e.g. Karlik and Winer, 2001).  
6 The broad range of temperatures encountered in different flights (mean range 21 – 33 °C) was  
7 responsible for quantitative differences in concentrations over the overlapping segments. The  
8 actual concentration at the surface can be significantly higher than observed at aircraft height,  
9 as is shown to be the case when flying near the tall tower at Walnut Grove where the top  
10 levels (394 and 525 m) saw very tiny concentration of isoprene consistent with the  
11 concentrations seen by aircraft although the lowest tower levels (10 and 131 m) saw much  
12 higher concentrations (Figure 6). However, the areas with significant biogenic emissions of  
13 isoprene covered a relatively small fetch within the footprint of the Walnut Grove tower.

14

15 The Twin Otter flew close to the WGC tower on RF2 and RF4 (13:18). The WGC region is  
16 mostly agricultural with a variety of sparsely distributed trees. The measurement during the  
17 aircraft pass at 13:18 showed very little isoprene (below 50 ppt) in excellent agreement with  
18 simultaneous observations at the top level (525 m) of the tower, even though concentrations  
19 around 1 ppb were observed at the 10 m level.

20

### 21 **3.2 Observed fluxes of isoprene from PTR-MS**

22 In this paper we focus on reporting isoprene surface fluxes.

23 The observed surface emission rates of isoprene over oak woodlands ranged from around 1 to  
24  $15 \text{ mg m}^{-2} \text{ h}^{-1}$ . The measured isoprene flux distribution shown in Figure 7 (CWT fluxes, 2 km  
25 resolution) visually confirms earlier predictions that isoprene emissions are almost  
26 exclusively produced by oak with a limited contribution from eucalyptus trees. For example,  
27 when entering the Sierra Nevada foothill oak band, isoprene emissions rose remarkably  
28 above the low background ( $0\text{-}0.05 \text{ mg m}^{-2} \text{ h}^{-1}$ ) in the Central Valley of California. The fact  
29 that isoprene is low over the Central Valley in midday at aircraft altitude does not necessarily  
30 mean that regional isoprene emissions are not important for photochemistry in the Central

1 Valley. Isoprene produced by the oaks surrounding the Central Valley gets oxidized during  
2 the daytime and its oxidation products such as MVK and MACR can be transported and then  
3 may be important for photochemistry when reacting in the presence of anthropogenic  
4 pollutants such as NO<sub>x</sub> leading to regional ozone and SOA formation. Figure 6 demonstrates  
5 the case within the Central Valley where local vegetation is patchy and sparse so isoprene  
6 concentration is very low at the aircraft altitude during midday, even though isoprene is  
7 observed to be much more abundant near the surface, and in the later afternoon. When the  
8 aircraft was passing the tower both the tower's top two inlet levels and the aircraft observed  
9 very low but non-zero concentrations of isoprene and MVK+MAC. However, the tower data  
10 demonstrate that oxidation products of isoprene routinely accumulate at night in the residual  
11 layer due to transport from the surrounding foothills where emissions are high. These high  
12 concentrations of isoprene oxidation products above the inversion layer are vented down in  
13 the morning when enough surface heating has occurred to cause vertical convection (Figure  
14 6). Thus previous studies inferring low significance of isoprene in the Central Valley might  
15 not account for this influence of isoprene emission from the surrounding foothills in the  
16 nighttime residual layer and in the morning when it is mixed vertically, and could therefore  
17 likely underplay the role of its oxidation products for regional photochemistry. Thus, to  
18 quantify the isoprene emission rates the daytime aircraft flux data are critical, but to  
19 understand the impact of isoprene emission in the Central Valley, a combination of the tower  
20 and aircraft observations are more useful than the daytime aircraft measurements alone. The  
21 extensive oak savannas are strong sources of isoprene. They grow with different area fraction  
22 cover and LAI and their regional characterization is crucial for understanding the magnitudes  
23 and extent to which these ecosystems contribute to the regional fluxes and the resulting  
24 distribution of oxidation products and photochemistry.

25 Karlik and McKay (2002) used an isoprene emission factor from branch enclosure for blue  
26 oak of  $27 \mu\text{g g}^{-1} \text{h}^{-1}$ , and leaf areas and weights from 14 blue oak trees from Sierra Nevada to  
27 estimate a leaf-level emission factor of  $\sim 8 \text{ mg m}^{-2}(\text{leaf}) \text{h}^{-1}$ , corresponding to a landscape  
28 emission factor of  $\sim 4 \text{ mg m}^{-2}(\text{land}) \text{h}^{-1}$  for a setting where oaks occupied half of the land  
29 surface area. In CABERNET the airborne emission factors for isoprene over oak woodlands  
30 varied from less than 1 to  $\sim 10 \text{ mg m}^{-2} \text{h}^{-1}$  with the average EF comprising all the flights over  
31 areas with oak presence ( $\geq 20\%$  coverage of oak species according to GAP database) of  $1.8$   
32  $\text{mg m}^{-2} \text{h}^{-1}$ . However, the woodlands varied in species homogeneity, and more significantly,

1 in the fraction (i.e., sparseness and patchiness) of tree coverage. It is necessary to emphasize  
2 that while the LAI of oak covered land surfaces has a relatively small range, about 3 to 6 m<sup>2</sup>  
3 m<sup>-2</sup>, the fraction of the land surface covered by oaks can range from < 0.1 to 1. For example,  
4 Karlik and McKay (2002) using a precise method of calculating the areas of leaves from 14  
5 trees divided by the areas of their crowns, measured an LAI of 4.3 m<sup>2</sup> m<sup>-2</sup> for oak crown areas  
6 but the oaks only covered 42% of the land surface resulting in an area average LAI of 1.8 m<sup>2</sup>  
7 m<sup>-2</sup>. For the more sparse terrains the area average LAI can often be lower than 1 m<sup>2</sup> m<sup>-2</sup>.  
8 Compared with the forests with closed canopies, modeling emissions from oak woodlands in  
9 California can be regarded as a specific case to which assessment by airborne flux  
10 measurements are particularly applicable. Measured airborne emissions reflect the true  
11 emissions from these California ecosystems of variable LAI ranging from less than 1 to about  
12 5 m<sup>2</sup> m<sup>-2</sup>.

13

14 Particularly strong isoprene emission hotspots were observed from the dense savannahs on  
15 the Sierra Nevada foothills dominated by Blue Oaks where ecosystem BEFs often exceeded 4  
16 mg m<sup>-2</sup> h<sup>-1</sup>. This oak band is continuous over approx. 800 km starting on the NE side of the  
17 valley from above Redding down through the east of Bakersfield and then tapers off before  
18 Lancaster. Going East towards the Sierras, for example towards the long term Blodgett  
19 measurement site (Goldstein et al., 2000), the emission factors degrade to around 1 mg m<sup>-2</sup> h<sup>-1</sup>  
20 or less as the ecosystem becomes conifer-dominated with only some oak trees remaining.  
21 Less homogenous isoprene source distribution were observed on the other side of the Central  
22 Valley near the coast and at the foothills and above Pacific Coast Ranges Mountains.  
23 Although Geron et al. (2001) found that blue oaks, coastal oaks and valley oaks have similar  
24 leaf level emission factors (within about 15%), these aircraft measurements indicate that  
25 regions where blue oaks mix with coastal oaks and valley oaks have higher isoprene  
26 emissions with observed ecosystem BEFs approaching 10 mg m<sup>-2</sup> h<sup>-1</sup>. As the wind blows  
27 from the coast it brings oxidation products to the urban areas in the Central Valley as well as  
28 the San Francisco Bay Area. In terms of the air quality of those regions, attention is generally  
29 focused on vehicle traffic and other anthropogenic emissions and the society is mostly  
30 unaware how important the oak-derived secondary products may be in secondary ozone  
31 formation which is driven by a combination of BVOCs and fossil fuel emissions (Steiner et  
32 al., 2006). Until now data on isoprene emissions in these regions have been completely

1 unavailable, and our airborne measurements clearly show where the emission hotspots are  
2 and what magnitudes of isoprene emissions are occurring in these regions close to highly  
3 populated cities of California. The distribution of emissions observed near these populated  
4 regions with serious air quality problems will be critical for assessing the true significance of  
5 isoprene emissions and its oxidation products for air pollution in areas commonly considered  
6 to be dominated by anthropogenic emissions.

7

### 8 3.2.1 Comparison of isoprene fluxes at Tonzi Ranch Tower

9 The aircraft flew over the Tonzi Ranch Tower twice, allowing two snapshot comparisons  
10 between the airborne CWT and ground based REA flux measurements. It is important to note  
11 that the airborne CWT averages over ~0.5 minute (2 km), while the ground based REA  
12 averages over 30 minutes, and that the footprints related to each measurement are necessarily  
13 quite different, likely do not have the same oak biomass density, and thus the comparison is  
14 not expected to be perfect. In the first instance, the half-hourly REA flux was in excellent  
15 agreement with the 2-km average wavelet surface flux over the tower (i.e.  $0.12 \pm 0.06 \text{ mg m}^{-2}$   
16  $\text{h}^{-1}$  REA vs  $0.12 \pm 0.06 \text{ mg m}^{-2} \text{ h}^{-1}$  aircraft) while on the returning flight the ground based flux  
17 was 1/3 of the aircraft flux (i.e.  $0.26 \pm 0.13 \text{ mg m}^{-2} \text{ h}^{-1}$  REA vs  $0.87 \pm 0.44 \text{ mg m}^{-2} \text{ h}^{-1}$ ).  
18 Interestingly, the next half-hour REA flux was  $0.96 \pm 0.48 \text{ mg m}^{-2} \text{ h}^{-1}$ , much closer to the  
19 aircraft value. This may be due to a shift in wind direction and variability in oak biomass  
20 density around the tower but it should also be noted that the uncertainty in a single REA flux  
21 measurement is high and individual values are typically averaged to improve accuracy.  
22 These comparisons obviously suffer from significant uncertainties due to different footprints  
23 at different altitudes, different temporal coverage, and even temperature/PAR homogeneities.  
24 Nevertheless, the comparison provides insight about the variability in measurements at  
25 different scales, confirms observations at these scales are in a similar range, and indicates  
26 how airplane and tower measurements are complementary. A larger period of overlap in a  
27 future campaign is needed for gaining better statistics on such comparisons.

28

### 3.2.2 Comparison of isoprene emission factors to MEGAN landcover 2.2

Isoprene emission model estimates are based on basal emission rates, landcover characteristics, and the changes in emission associated with the environmental parameters temperature and photosynthetically active radiation (PAR). The airborne surface flux normalized for temperature and radiation using the Guenther et al. (2006) activity factor can be used to derive airborne basal emission factors (BEFs) to directly compare to emission factors used by models (e.g. the MEGAN emission factors version 2.2). A spatial comparison is shown in Figure 7. It needs to be noted that such an approach introduces additional uncertainty from the temperature and PAR datasets and the algorithm used for calculating the activity coefficient, which are much higher than the uncertainty of the measured surface fluxes because of high sensitivity to errors in temperature and PAR. For this reason, in this manuscript we treat this comparison as semi-quantitative, and will explore this in more detail as part of another paper (Misztal et al., 2014) which focuses on using the airborne data to examine the accuracy of several different BVOC emission models, including detailed sensitivity analyses and input data validation. However, the qualitative picture clearly shows the remarkable correspondence of airborne BEFs derived at 2 km spatial resolution with landcover BEFs at a similar resolution. The transition from the low emitting environment in the Central Valley to highly emitting areas occupied by oak woodlands is clear (as shown earlier in Figure 1). The most accurate match can be seen, for example, in the central part of the Sierra foothills and on the southern Coastal Range, to the south east of Monterey Bay and in the oak savannas near San Francisco Bay (Orinda, and Diablo Valley). The BEFs decline to zero over water bodies (e.g. San Francisco Bay, or lakes on the central-northern Sierras). There are some areas which do not agree well, for example, in the north-east over the Sierras which are dominated by conifers where airborne BEFs were somewhat lower. On the other hand, the areas where aircraft showed higher BEFs (e.g. beginning of RF8) are most likely related to inaccuracies in the oak landcover database. For the first time it is now possible to constrain the emission estimates generated by models using direct airborne observations on scales relevant for these models, and to examine how best to improve modeling approaches including more accurate driving variables and landcover.

## 1 4 Conclusions

2 We successfully performed airborne eddy covariance flux measurements and mapped out  
3 horizontally varying source distributions of isoprene emissions for the dominant oak emitting  
4 ecosystems in California. The extensive oak woodlands in California are the most important  
5 regional source of isoprene which may be particularly relevant for the photochemistry and air  
6 quality near heavily polluted regions of the Central Valley, but also other areas surrounded by  
7 substantial areas of oak woodlands including much of the San Francisco Bay Area. We  
8 observed high concentrations (up to 8 ppbv) and high surface emissions of isoprene ranging  
9 from several to more than  $10 \text{ mg m}^{-2} \text{ h}^{-1}$  from the oak woodlands in the foothills of the Sierra  
10 Nevada and Coastal Ranges. Consistent with other studies we show that in the Central Valley  
11 isoprene emissions are typically undetectably small at aircraft level except for the areas of  
12 Eucalyptus trees planted near the highways. However, using the combination of aircraft and  
13 tall tower measurements we point out that isoprene chemistry may still play an important role  
14 even in those areas where midday isoprene fluxes and concentrations are low, because  
15 substantial amounts of isoprene-oxidation products are transported from the surrounding  
16 areas which have high emissions and collect in the residual layer at night, mixing down to the  
17 surface in the morning. Furthermore, the tower measurements show us that there are at least  
18 small isoprene emissions occurring in the valley but the rapid oxidation during the day makes  
19 the relatively small emissions from the from Central Valley hard to observe at aircraft height.  
20 The temperature ranges in California cause changes in the isoprene emissions from relatively  
21 low to extremely high due to their strong temperature sensitivity and our flights were  
22 performed in early summer season before the highest emissions are expected. The ability of  
23 CWT for calculating fluxes at high spatial resolution provides an optimal data set to compare  
24 BEFs independent of environmental conditions from measurements with models. The data  
25 from this study will be used to assess isoprene emission-factor databases and isoprene  
26 emission response to landcover characteristics predicted for BVOC emission models. The  
27 ability to measure direct airborne fluxes over heterogeneous landscapes was needed to  
28 improve landcover descriptions in biogenic emission models. This dataset on isoprene fluxes  
29 will be particularly useful for evaluating potential model alternatives which will be dealt with  
30 in a separate paper to assess isoprene emission models and their driving variable datasets.

31



1 **Acknowledgements**

2 We gratefully acknowledge California Air Resources Board (CARB) for funding  
3 CABERNET Contract #09-339 and Walnut Grove Contract #11-315, and the CIRPAS team  
4 for help in instrument integration. We acknowledge Abhinav Guha (UC Berkeley) for his  
5 contributions to the successful campaign. Finally, we would like to thank Andrew  
6 Turnipseed (NCAR) and Tiffany Duhl (NCAR) for performing GC analyses of aircraft  
7 cartridges, and Steve Shertz (NCAR) for engineering support. NCAR is sponsored by the  
8 National Science Foundation. Alex Guenther was partly funded under the Laboratory  
9 Directed Research and Development Program at PNNL, a multi-program national laboratory  
10 operated by Battelle for the U.S. Department of Energy under Contract DE-AC05-  
11 76RL01830. We also acknowledge Prof. Maggi Kelly at GIF, UC Berkeley for suggestions  
12 regarding geospatial landcovers. We thank Jeremy Avise and Klaus Scott at California Air  
13 Resources Board for collaboration and useful modeling suggestions.

14

## 1 **References**

- 2 Apel, E., Riemer, D., Hills, A., Baugh, W., Orlando, J., Faloona, I., Tan, D., Brune, W.,  
3 Lamb, B., and Westberg, H.: Measurement and interpretation of isoprene fluxes and isoprene,  
4 methacrolein, and methyl vinyl ketone mixing ratios at the PROPHET site during the 1998  
5 Intensive, *Journal of Geophysical Research*, 107, 4034, 2002.
- 6 Arey, J., Corchnoy, S. B., and Atkinson, R.: Emission of linalool from Valencia orange  
7 blossoms and its observation in ambient air, *Atmos Environ a-Gen*, 25, 1377-1381, 1991.
- 8 Arey, J., Crowley, D. E., Crowley, M., Resketo, M., and Lester, J.: Hydrocarbon Emissions  
9 from Natural Vegetation in California South-Coast-Air-Basin, *Atmospheric Environment*, 29,  
10 2977-2988, Doi 10.1016/1352-2310(95)00137-N, 1995.
- 11 Baker, B., Guenther, A., Greenberg, J., Goldstein, A., and Fall, R.: Canopy fluxes of 2-  
12 methyl-3-buten-2-ol over a ponderosa pine forest by relaxed eddy accumulation: Field data  
13 and model comparison, *J Geophys Res-Atmos*, 104, 26107-26114, Doi  
14 10.1029/1999jd900749, 1999.
- 15 Baldocchi, D. D.: Assessing the eddy covariance technique for evaluating carbon dioxide  
16 exchange rates of ecosystems: past, present and future, *Global Change Biol*, 9, 479-492,  
17 2003.
- 18 Bange, J., Zittel, P., Spiess, T., Uhlenbrock, J., and Beyrich, F.: A new method for the  
19 determination of area-averaged turbulent surface fluxes from low-level flights using inverse  
20 models, *Boundary-Layer Meteorology*, 119, 527-561, DOI 10.1007/s10546-005-9040-6,  
21 2006.
- 22 Claussen, M.: Area-Averaging of Surface Fluxes in a Neutrally Stratified, Horizontally  
23 Inhomogeneous Atmospheric Boundary-Layer, *Atmos Environ a-Gen*, 24, 1349-1360, Doi  
24 10.1016/0960-1686(90)90041-K, 1990.
- 25 Desjardins, R. L., Hart, R. L., Macpherson, J. I., Schuepp, P. H., and Verma, S. B.: Aircraft-  
26 Based and Tower-Based Fluxes of Carbon-Dioxide, Latent, and Sensible Heat, *J Geophys  
27 Res-Atmos*, 97, 18477-18485, 1992.
- 28 Fares, S., Gentner, D. R., Park, J. H., Ormeno, E., Karlik, J., and Goldstein, A. H.: Biogenic  
29 emissions from Citrus species in California, *Atmospheric Environment*, 45, 4557-4568, DOI  
30 10.1016/j.atmosenv.2011.05.066, 2011.
- 31 Fares, S., Park, J. H., Gentner, D. R., Weber, R., Ormeno, E., Karlik, J., and Goldstein, A. H.:  
32 Seasonal cycles of biogenic volatile organic compound fluxes and concentrations in a  
33 California citrus orchard, *Atmos Chem Phys*, 12, 9865-9880, DOI 10.5194/acp-12-9865-  
34 2012, 2012.
- 35 Fuentes, J. D., and Wang, D.: On the seasonality of isoprene emissions from a mixed  
36 temperate forest, *Ecological Applications*, 9, 1118-1131, Doi 10.2307/2641382, 1999.
- 37 Geron, C., Harley, P., and Guenther, A.: Isoprene emission capacity for US tree species,  
38 *Atmospheric Environment*, 35, 3341-3352, 2001.
- 39 Goldstein, A., Hultman, N., Fracheboud, J., Bauer, M., Panek, J., Xu, M., Qi, Y., Guenther,  
40 A., and Baugh, W.: Effects of climate variability on the carbon dioxide, water, and sensible  
41 heat fluxes above a ponderosa pine plantation in the Sierra Nevada (CA), *Agr Forest  
42 Meteorol*, 101, 113-129, 2000.

1 Goldstein, A. H., Goulden, M. L., Munger, J. W., Wofsy, S. C., and Geron, C. D.: Seasonal  
2 course of isoprene emissions from a midlatitude deciduous forest, *Journal of Geophysical*  
3 *Research: Atmospheres* (1984–2012), 103, 31045-31056, 1998.

4 Goldstein, A. H., and Schade, G. W.: Quantifying biogenic and anthropogenic contributions  
5 to acetone mixing ratios in a rural environment, *Atmospheric Environment*, 34, 4997-5006,  
6 Doi 10.1016/S1352-2310(00)00321-6, 2000.

7 Guenther, A., Karl, T., Harley, P., Wiedinmyer, C., Palmer, P. I., and Geron, C.: Estimates of  
8 global terrestrial isoprene emissions using MEGAN (Model of Emissions of Gases and  
9 Aerosols from Nature), *Atmos. Chem. Phys.*, 6, 3181-3210, 10.5194/acp-6-3181-2006, 2006.

10 Guenther, A. B., Jiang, X., Heald, C. L., Sakulyanontvittaya, T., Duhl, T., Emmons, L. K.,  
11 and Wang, X.: The Model of Emissions of Gases and Aerosols from Nature version 2.1  
12 (MEGAN2.1): an extended and updated framework for modeling biogenic emissions, *Geosci*  
13 *Model Dev*, 5, 1471-1492, DOI 10.5194/gmd-5-1471-2012, 2012.

14 Hegg, D. A., Covert, D. S., Jonsson, H., and Covert, P. A.: Determination of the transmission  
15 efficiency of an aircraft aerosol inlet, *Aerosol Sci Tech*, 39, 966-971, Doi  
16 10.1080/02786820500377814, 2005.

17 Karl, T., Guenther, A., Turnipseed, A., Patton, E. G., and Jardine, K.: Chemical sensing of  
18 plant stress at the ecosystem scale, *Biogeosciences*, 5, 1287-1294, 2008.

19 Karl, T., Apel, E., Hodzic, A., Riemer, D. D., Blake, D. R., and Wiedinmyer, C.: Emissions  
20 of volatile organic compounds inferred from airborne flux measurements over a megacity,  
21 *Atmos Chem Phys*, 9, 271-285, 2009.

22 Karl, T., Misztal, P. K., Jonsson, H. H., Shertz, S., Goldstein, A. H., and Guenther, A. B.:  
23 Airborne Flux Measurements of BVOCs above Californian Oak Forests: Experimental  
24 Investigation of Surface and Entrainment Fluxes, OH Densities, and Damkohler Numbers, *J*  
25 *Atmos Sci*, 70, 3277-3287, Doi 10.1175/Jas-D-13-054.1, 2013.

26 Karl, T. G., Spirig, C., Rinne, J., Stroud, C., Prevost, P., Greenberg, J., Fall, R., and  
27 Guenther, A.: Virtual disjunct eddy covariance measurements of organic compound fluxes  
28 from a subalpine forest using proton transfer reaction mass spectrometry, *Atmos Chem Phys*,  
29 2, 279-291, 2002.

30 Karlik, J. F., and Winer, A. M.: Measured isoprene emission rates of plants in California  
31 landscapes: comparison to estimates from taxonomic relationships, *Atmospheric*  
32 *Environment*, 35, 1123-1131, 2001.

33 Karlik, J. F., and McKay, A. H.: Leaf area index, leaf mass density, and allometric  
34 relationships derived from harvest of blue oaks in a California oak savanna, USDA Forest  
35 Service General Technical Report Number PSW-GTR-184, Albany, CA, 2002.

36 Kristensen, L., Mann, J., Oncley, S. P., and Wyngaard, J. C.: How close is close enough  
37 when measuring scalar fluxes with displaced sensors?, *J Atmos Ocean Tech*, 14, 814-821,  
38 Doi 10.1175/1520-0426(1997)014<0814:Hcicew>2.0.Co;2, 1997.

39 Kuhn, U., Rottenberger, S., Biesenthal, T., Wolf, A., Schebeske, G., Ciccioli, P., Brancaleoni,  
40 E., Frattoni, M., Tavares, T., and Kesselmeier, J.: Isoprene and monoterpene emissions of  
41 Amazonian tree species during the wet season: Direct and indirect investigations on  
42 controlling environmental functions, *Journal of Geophysical Research*, 107, 8071, 2002.

1 Kurpius, M. R., and Goldstein, A. H.: Gas-phase chemistry dominates O<sub>3</sub> loss to a forest,  
2 implying a source of aerosols and hydroxyl radicals to the atmosphere, *Geophys Res Lett*, 30,  
3 Artn 1371  
4 Doi 10.1029/2002gl016785, 2003.

5 Lamb, B., Westberg, H., and Allwine, G.: Isoprene Emission Fluxes Determined by an  
6 Atmospheric Tracer Technique, *Atmospheric Environment*, 20, 1-8, Doi 10.1016/0004-  
7 6981(86)90201-5, 1986.

8 Langford, B., Misztal, P. K., Nemitz, E., Davison, B., Helfter, C., Pugh, T. A. M.,  
9 MacKenzie, A. R., Lim, S. F., and Hewitt, C. N.: Fluxes and concentrations of volatile  
10 organic compounds from a South-East Asian tropical rainforest, *Atmos. Chem. Phys.*, 10,  
11 8391-8412, 10.5194/acp-10-8391-2010, 2010.

12 Lenschow, D. H., Delany, A. C., Stankov, B. B., and Stedman, D. H.: Airborne  
13 Measurements of the Vertical Flux of Ozone in the Boundary-Layer, *Boundary-Layer*  
14 *Meteorology*, 19, 249-265, Doi 10.1007/Bf00117223, 1980.

15 Lenschow, D. H., Pearson, R., and Stankov, B. B.: Estimating the Ozone Budget in the  
16 Boundary-Layer by Use of Aircraft Measurements of Ozone Eddy Flux and Mean  
17 Concentration, *J Geophys Res-Oc Atm*, 86, 7291-7297, 1981.

18 Lenschow, D. H.: Probing the Atmospheric Boundary Layer, *Probing the Atmospheric*  
19 *Boundary Layer*, American Meteorological Society, Boston, MA, 1986.

20 Loreto, F., and Sharkey, T. D.: A gas-exchange study of photosynthesis and isoprene  
21 emission in *Quercus rubra* L, *Planta*, 182, 523-531, 1990.

22 Mahrt, L.: Surface heterogeneity and vertical structure of the boundary layer, *Boundary-*  
23 *Layer Meteorology*, 96, 33-62, Doi 10.1023/A:1002482332477, 2000.

24 Mann, J., and Lenschow, D. H.: Errors in Airborne Flux Measurements, *J Geophys Res-*  
25 *Atmos*, 99, 14519-14526, Doi 10.1029/94jd00737, 1994.

26 Mason, P. J.: The Formation of Areally-Averaged Roughness Lengths, *Q J Roy Meteor Soc*,  
27 114, 399-420, DOI 10.1002/qj.49711448007, 1988.

28 Mauder, M., Desjardins, R. L., and MacPherson, I.: Scale analysis of airborne flux  
29 measurements over heterogeneous terrain in a boreal ecosystem, *J Geophys Res-Atmos*, 112,  
30 Artn D13112  
31 Doi 10.1029/2006jd008133, 2007.

32 Metzger, S., Junkermann, W., Mauder, M., Butterbach-Bahl, K., Trancón y Widemann, B.,  
33 Neidl, F., Schäfer, K., Wieneke, S., Zheng, X., and Schmid, H.: Spatially explicit  
34 regionalization of airborne flux measurements using environmental response functions,  
35 *Biogeosciences*, 10, 2193-2217, 2013.

36 Misztal, P. K., Avise, J., Karl, T., Scott, K., Weber, R., Jonsson, H. H., Guenther, A. B., and  
37 Goldstein, A. H.: Evaluation of regional isoprene emission estimates in California based on  
38 direct airborne flux measurements, In preparation for ACP, 2014.

39 Moore, C.: Frequency response corrections for eddy correlation systems, *Boundary-Layer*  
40 *Meteorology*, 37, 17-35, 1986.

- 1 Nordbo, A., and Katul, G.: A Wavelet-Based Correction Method for Eddy-Covariance High-  
2 Frequency Losses in Scalar Concentration Measurements, *Boundary-Layer Meteorology*,  
3 146, 81-102, 10.1007/s10546-012-9759-9, 2013.
- 4 Panofsky, H. A., and Dutton, J. A.: *Atmospheric turbulence: models and methods for*  
5 *engineering applications*, Wiley, New York, 1984.
- 6 Park, J.-H., Goldstein, A. H., Timkovsky, J., Fares, S., Weber, R., Karlik, J., and Holzinger,  
7 R.: Active Atmosphere-Ecosystem Exchange of the Vast Majority of Detected Volatile  
8 Organic Compounds, *Science*, 341, 643-647, 10.1126/science.1235053, 2013.
- 9 Pattey, E., Strachan, I., Desjardins, R., and Massheder, J.: Measuring nighttime CO<sub>2</sub> flux  
10 over terrestrial ecosystems using eddy covariance and nocturnal boundary layer methods, *Agr*  
11 *Forest Meteorol*, 113, 145-158, 2002.
- 12 Pierce, T., Geron, C., Bender, L., Dennis, R., Tonnesen, G., and Guenther, A.: Influence of  
13 increased isoprene emissions on regional ozone modeling, *J Geophys Res-Atmos*, 103,  
14 25611-25629, Doi 10.1029/98jd01804, 1998.
- 15 Rasmussen, R. A.: Isoprene: Identified as a forest-type emission to the atmosphere,  
16 *Environmental Science & Technology*, 4, 667-671, 1970.
- 17 Raupach, M. R., and Finnigan, J. J.: Scale Issues in Boundary-Layer Meteorology - Surface-  
18 Energy Balances in Heterogeneous Terrain, *Hydrol Process*, 9, 589-612, DOI  
19 10.1002/hyp.3360090509, 1995.
- 20 Reid, J. S., Jonsson, H. H., Smith, M. H., and Smirnov, A.: Evolution of the vertical profile  
21 and flux of large sea-salt particles in a coastal zone, *J Geophys Res-Atmos*, 106, 12039-  
22 12053, Doi 10.1029/2000jd900848, 2001.
- 23 Rinne, H., Guenther, A., Greenberg, J., and Harley, P.: Isoprene and monoterpene fluxes  
24 measured above Amazonian rainforest and their dependence on light and temperature,  
25 *Atmospheric Environment*, 36, 2421-2426, 2002.
- 26 Rowe, M. D., Fairall, C. W., and Perlinger, J. A.: Chemical sensor resolution requirements  
27 for near-surface measurements of turbulent fluxes, *Atmos. Chem. Phys.*, 11, 5263-5275,  
28 10.5194/acp-11-5263-2011, 2011.
- 29 Schade, G. W., Goldstein, A. H., and Lamanna, M. S.: Are monoterpene emissions  
30 influenced by humidity?, *Geophys Res Lett*, 26, 2187-2190, Doi 10.1029/1999gl900444,  
31 1999.
- 32 Schade, G. W., Goldstein, A. H., Gray, D. W., and Lerdau, M. T.: Canopy and leaf level 2-  
33 methyl-3-buten-2-ol fluxes from a ponderosa pine plantation, *Atmospheric Environment*, 34,  
34 3535-3544, Doi 10.1016/S1352-2310(00)00120-5, 2000.
- 35 Schade, G. W., and Goldstein, A. H.: Fluxes of oxygenated volatile organic compounds from  
36 a ponderosa pine plantation, *J Geophys Res-Atmos*, 106, 3111-3123, Doi  
37 10.1029/2000jd900592, 2001.
- 38 Scott, K. I., and Benjamin, M. T.: Development of a biogenic volatile organic compounds  
39 emission inventory for the SCOS97-NARSTO domain, *Atmospheric Environment*, 37, S39-  
40 S49, Doi 10.1016/S1352-2310(03)00381-9, 2003.
- 41 Serca, D., Guenther, A., Klinger, L., Vierling, L., Harley, P., Druilhet, A., Greenberg, J.,  
42 Baker, B., Baugh, W., Bouka-Biona, C., and Loemba-Ndembu, J.: EXPRESSO flux

- 1 measurements at upland and lowland Congo tropical forest site, *Tellus B*, 53, 220-234, DOI  
2 10.1034/j.1600-0889.2001.01237.x, 2001.
- 3 Sharkey, T. D., Singsaas, E. L., Lerdau, M. T., and Geron, C. D.: Weather effects on isoprene  
4 emission capacity and applications in emissions algorithms, *Ecological Applications*, 9,  
5 1132-1137, 1999.
- 6 Steiner, A., Pressley, S., Botros, A., Jones, E., Chung, S., and Edburg, S.: Analysis of  
7 coherent structures and atmosphere-canopy coupling strength during the CABINEX field  
8 campaign, *Atmos Chem Phys*, 11, 11921-11936, 2011.
- 9 Steiner, A. L., Tonse, S., Cohen, R. C., Goldstein, A. H., and Harley, R. A.: Influence of  
10 future climate and emissions on regional air quality in California, *Journal of Geophysical  
11 Research: Atmospheres* (1984–2012), 111, D18303, 10.1029/2005JD006935, 2006.
- 12 Stoy, P. C., Richardson, A. D., Baldocchi, D. D., Katul, G. G., Stanovick, J., Mahecha, M.  
13 D., Reichstein, M., Detto, M., Law, B. E., Wohlfahrt, G., Arriga, N., Campos, J.,  
14 McCaughey, J. H., Montagnani, L., Paw U, K. T., Sevanto, S., and Williams, M.: Biosphere-  
15 atmosphere exchange of CO<sub>2</sub> in relation to climate: a cross-biome analysis across multiple  
16 time scales, *Biogeosciences*, 6, 2297-2312, 10.5194/bg-6-2297-2009, 2009.
- 17 Thomas, C., and Foken, T.: Detection of long-term coherent exchange over spruce forest  
18 using wavelet analysis, *Theor Appl Climatol*, 80, 91-104, 2005.
- 19 Thomas, C., and Foken, T.: Flux contribution of coherent structures and its implications for  
20 the exchange of energy and matter in a tall spruce canopy, *Boundary-Layer Meteorology*,  
21 123, 317-337, DOI 10.1007/s10546-006-9144-7, 2007.
- 22 Torrence, C., and Compo, G. P.: A practical guide to wavelet analysis, *B Am Meteorol Soc*,  
23 79, 61-78, 1998.
- 24 Vargas, R., Detto, M., Baldocchi, D. D., and Allen, M. F.: Multiscale analysis of temporal  
25 variability of soil CO<sub>2</sub> production as influenced by weather and vegetation, *Global Change  
26 Biol*, 16, 1589-1605, 2010.
- 27 Weil, J. C., and Horst, T. W.: Footprint Estimates for Atmospheric Flux Measurements in the  
28 Convective Boundary-Layer, *Precipitation Scavenging and Atmosphere-Surface Exchange*,  
29 Vols 1-3, 717-728, 1992.
- 30 Westberg, H., Lamb, B., Hafer, R., Hills, A., Shepson, P., and Vogel, C.: Measurement of  
31 isoprene fluxes at the PROPHET site, *Journal of Geophysical Research: Atmospheres* (1984–  
32 2012), 106, 24347-24358, 2001.
- 33 Winer, A. M., Arey, J., Atkinson, R., Aschmann, S. M., Long, W. D., Morrison, C. L., and  
34 Olszyk, D. M.: Emission Rates of Organics from Vegetation in California Central Valley,  
35 *Atmos Environ a-Gen*, 26, 2647-2659, Doi 10.1016/0960-1686(92)90116-3, 1992.
- 36 Wood, N., and Mason, P.: The Influence of Static Stability on the Effective Roughness  
37 Lengths for Momentum and Heat-Transfer, *Q J Roy Meteor Soc*, 117, 1025-1056, DOI  
38 10.1002/qj.49711750108, 1991.
- 39 Wyngaard, J. C., and Brost, R. A.: Top-down and bottom-up diffusion of a scalar in the  
40 convective boundary layer, *J Atmos Sci*, 41, 102-112, 1984.

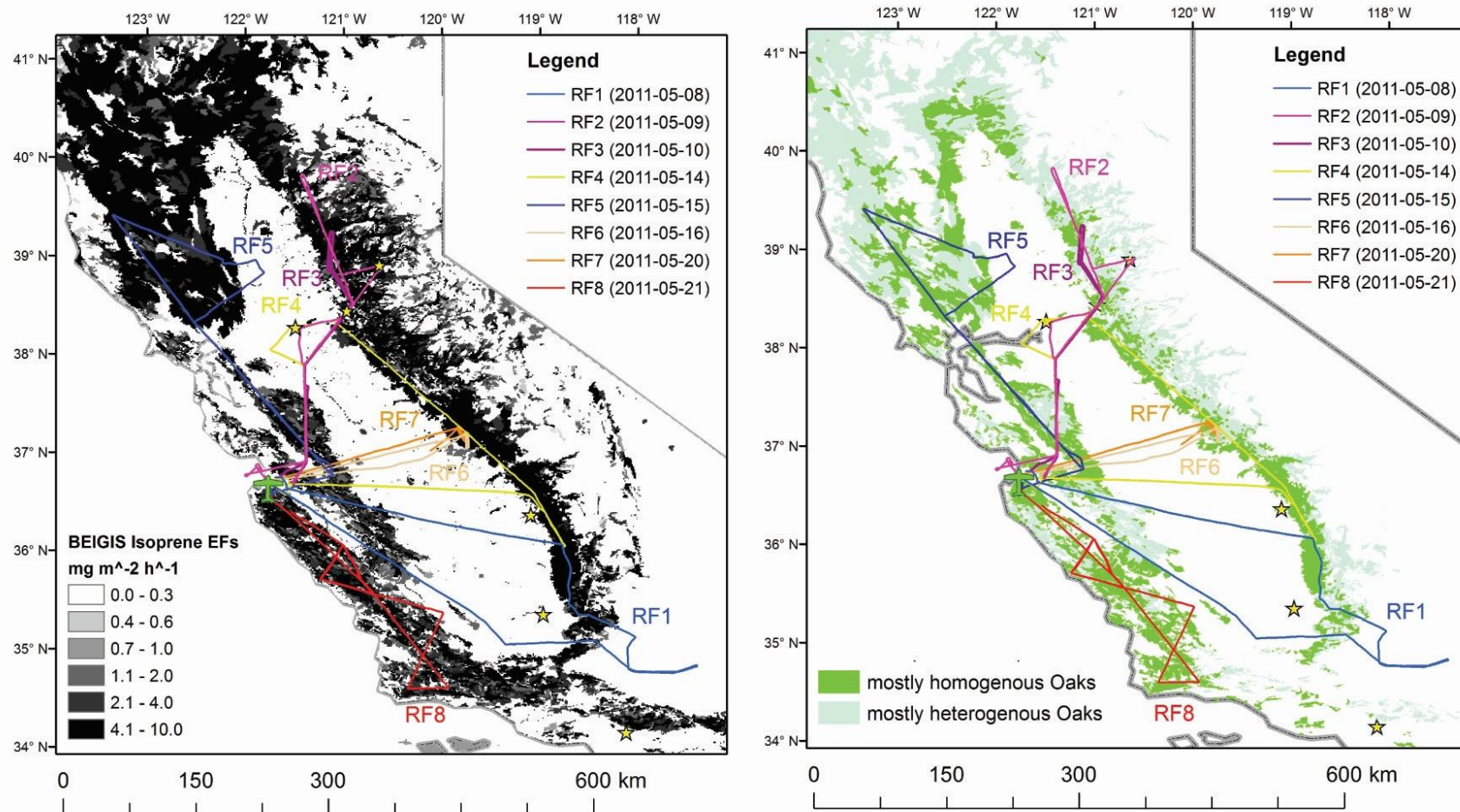
41  
42  
43

1

2 Table 1. Selected flight parameter data specific to each research flight

	RF1 June 8	RF2 June 9	RF3 June 10	RF4 June 14	RF5 June 15	RF6 June 16	RF7 June 20	RF8 June 21
Temperature close to the surface (2 m WRF) (°C)								
mean (median)	20.6 (21.5)	23.1 (23.8)	24.4 (25.3)	27.8 (28.6)	28.5 (29.4)	24.8 (25.4)	29.7 (30.3)	32.5 (33.4)
s.d.	3.21	3.21	3.46	2.88	3.24	3.96	2.64	3.54
min	11.3	10.9	11.4	11.7	12.2	11.8	12.1	11.7
max	25.9	28.0	29.6	32.1	33.8	31.4	34.9	37.2
5 <sup>th</sup> percentile	14.4	17.1	17.7	23.4	22.6	16.8	26.0	27.0
95 <sup>th</sup> percentile	24.6	27.1	28.5	31.1	32.3	29.6	32.4	36.0
Altitude (m a.g.l.)								
mean (median)	603 (437)	551 (449)	831 (685)	529 (470)	511 (489)	836 (721)	852 (730)	462 (396)
s.d.	436	309	575	233	193	461	565	210
min	127	119	126	209	127	55.3	50.0	160
max	2410	1830	2790	1720	1460	2610	1870	1540
5 <sup>th</sup> percentile	251	266	285	301	278	291	289	268
95 <sup>th</sup> percentile	1670	1300	2090	949	712	1640	1830	887
Convective velocity scale <sup>a</sup> , $w^*$ (m/s)								
mean (median)	4.40 (4.42)	3.56 (3.46)	3.19 (2.94)	3.20 (3.21)	2.61 (2.47)	3.62 (3.61)	3.42 (3.43)	2.86 (2.62)
s.d.	1.55	0.92	1.19	1.01	0.79	1.12	0.85	1.11
min	1.18	1.64	1.27	1.18	0.84	1.72	2.2	1.12
max	8.25	8.69	8.13	5.72	5.11	6.25	4.95	5.87
5 <sup>th</sup> percentile	1.87	2.22	1.54	1.62	1.46	1.99	2.31	1.33
95 <sup>th</sup> percentile	7.01	5.12	5.25	4.67	4.10	5.58	4.82	4.99
Other flight characteristics								
Take off time UTC (local/PDT)	17:30 (11:30)	18:15 (12:15)	18:10 (12:10)	18:05 (12:05)	18:00 (12:00)	19:05 (13:05)	19:05 (13:05)	18:55 (12:55)
Touchdown time UTC (local/PDT)	22:20 (16:20)	22:45 (16:45)	22:10 (16:10)	22:35 (16:35)	22:30 (16:30)	0:05 (18:05)	00:30 (18:30)	23:30 (17:30)
Flight focus	Survey	Survey	Survey, Racetrack	Survey	Survey	Racetrack	Racetrack	Survey
Total length (km)	983	908	802	896	875	1020	835	935
PBL height range (km)	0.9 - 2.8	1.4 - 1.7	0.8-1.1	0.4-1.9	1.1-1.1	1.6-1.7	1.2-1.2	0.7-1.4
VOC-related $m/z$ measured (10 Hz) <sup>b</sup>	69, 33, 79, 93, 107	69, 71, 33, 81, 137, 87	69, 71, 75, 33	69, 71, 33, 81, 137, 87	69, 71, 33, 81, 137, 45	69, 71, 87	69, 71, 75	69, 71, 33, 137, 87

3 <sup>a</sup>approximated from wavelet heat fluxes (uncorrected) on survey tracks (including only the lowest racetrack levels);  
<sup>b</sup> $m/z$  21, 32, and 37 were also measured on every flight at 10, 20 and 20 Hz respectively.

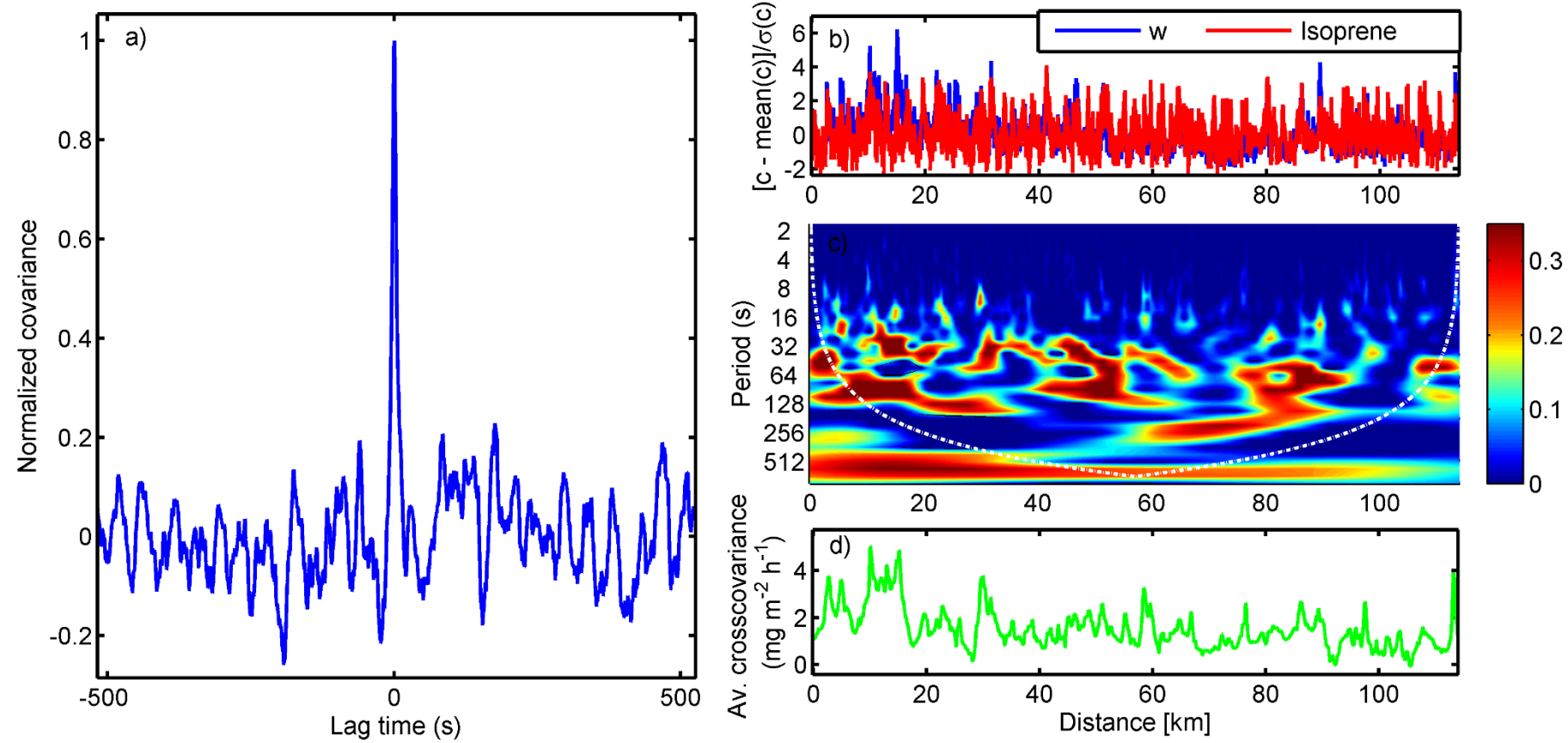


1

2 Figure 1. Tracks flown during CABERNET overlaid over (a) BEIGIS Isoprene Emission Factor (EF) landcover; and (b) oak-woodland ecosystems differing in oak species  
 3 spatial homogeneity (according to the GAP database).



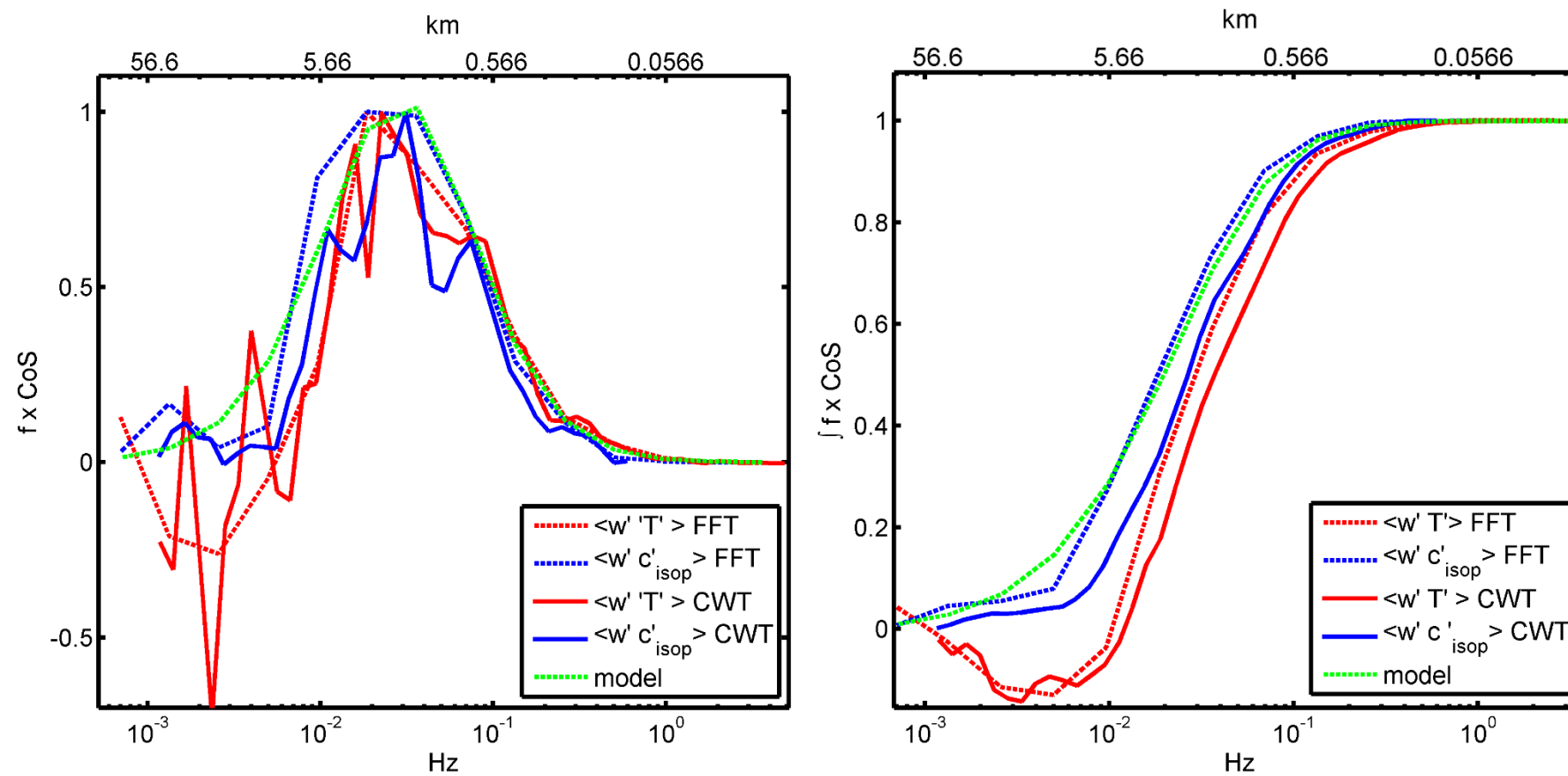
1



2

3 Figure 2. Flux quality control for an example flight leg (the segment from Supplementary Fig. S2). a) Clear peak in the covariance  
4 function; b) variances of  $w$  and isoprene; c) time-resolved wavelet co-spectra; and d) average cross-variance.

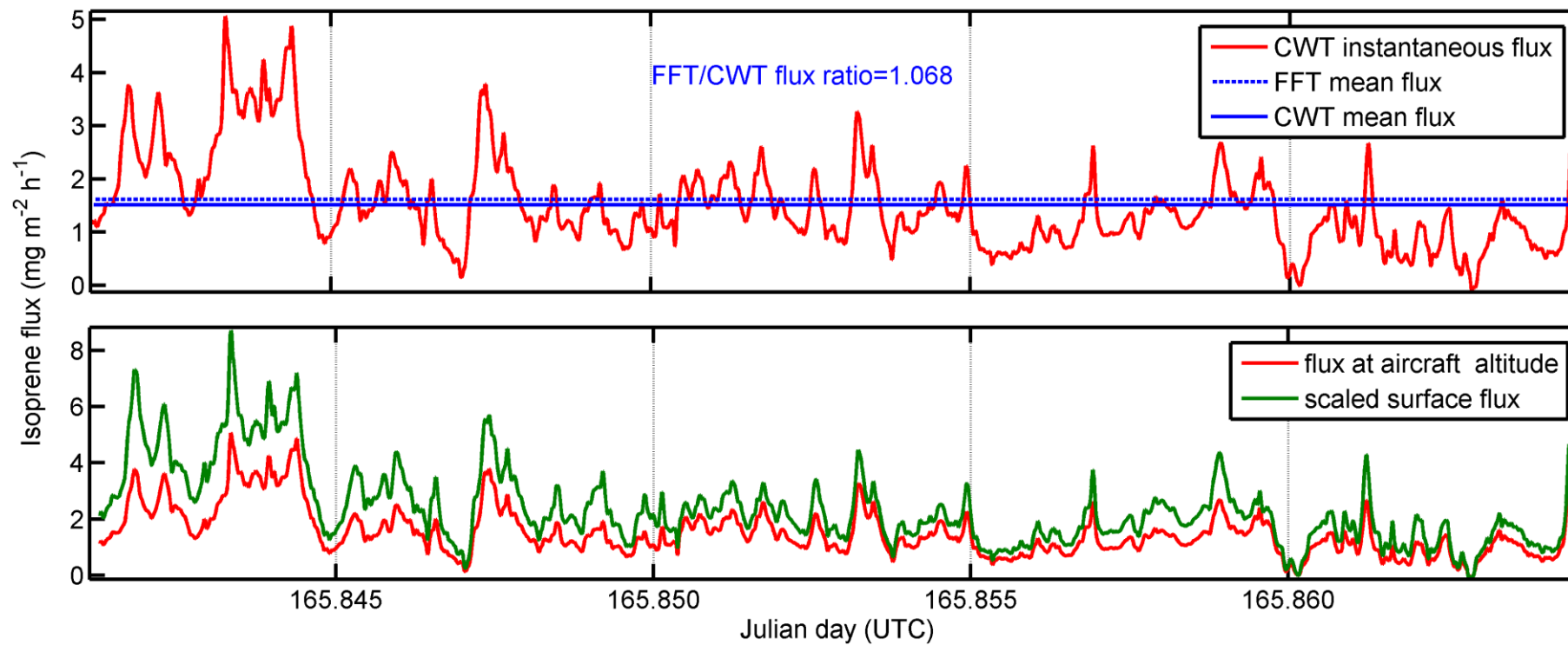
1  
2



3  
4

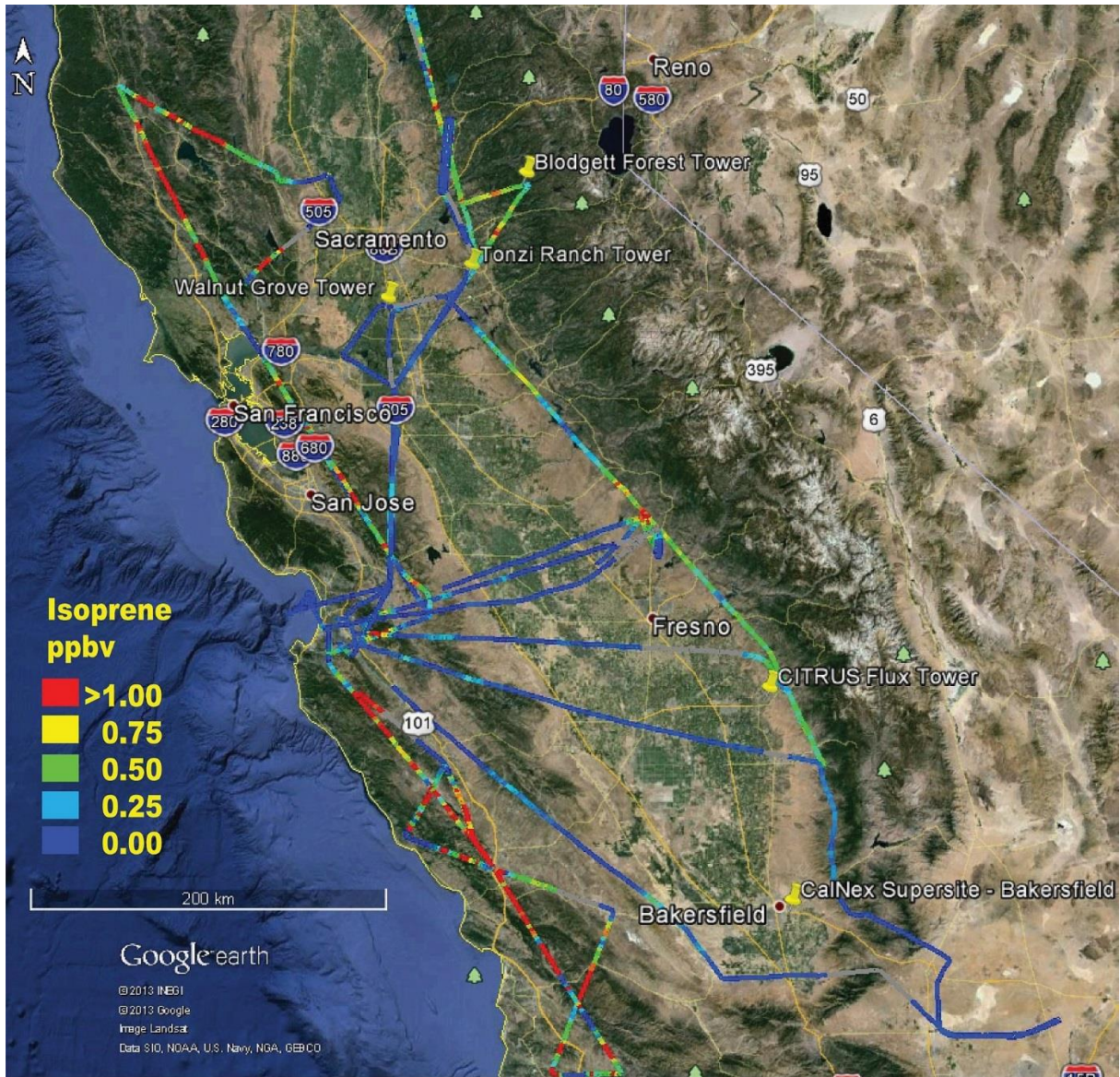
Figure 3. Spectral quality control of the example flight segment. Left panel: Comparison of co-spectra for isoprene flux and heat flux using the FFT and CWT methods independently; Right panel: Cumulative co-spectra for isoprene flux and heat flux using the FFT and CWT methods independently. The green lines in left and right panels show the model that is used with transfer functions optimized from Kristensen et al. (1997).

1  
2



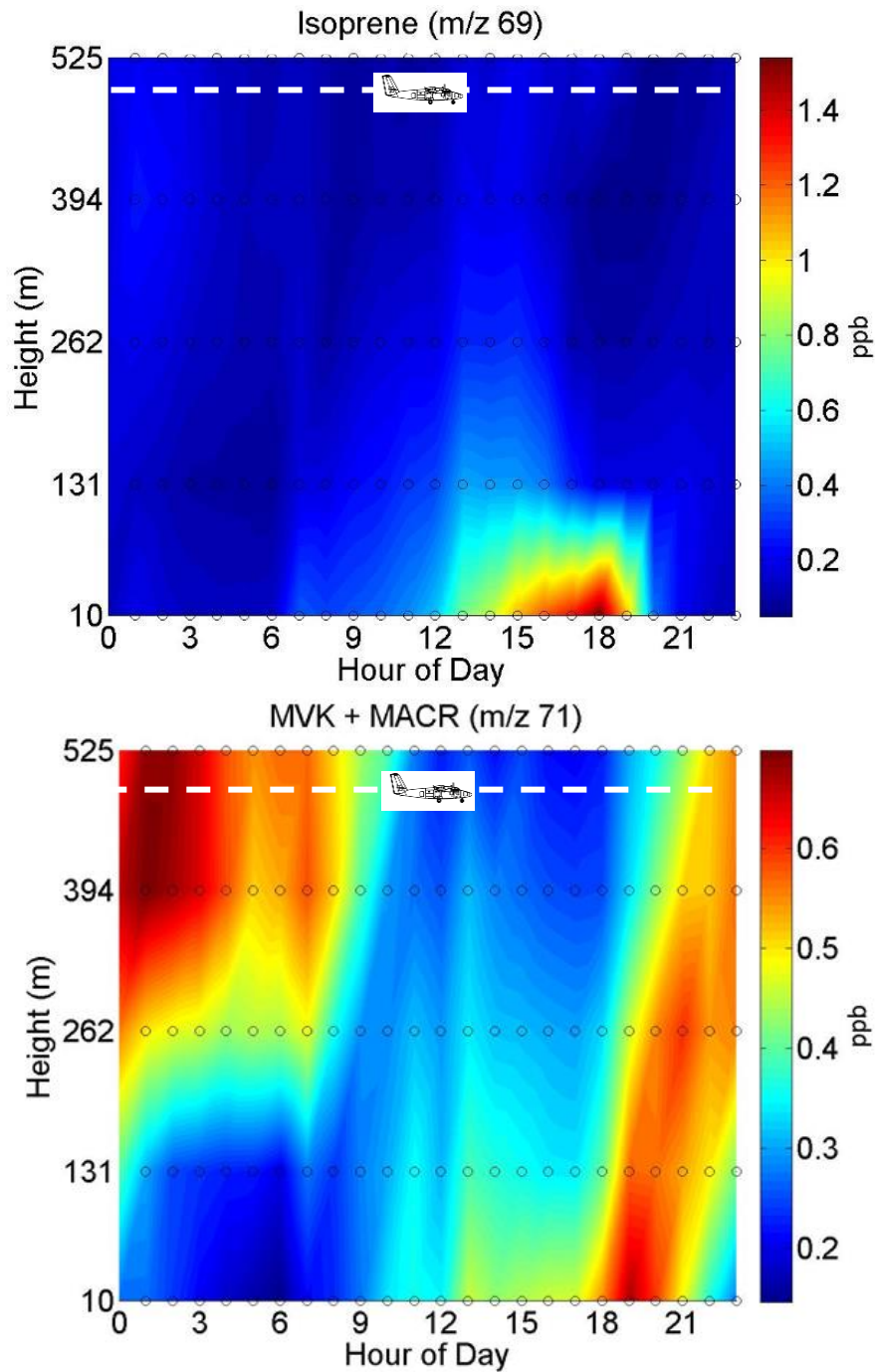
3  
4  
5

Figure 4. Isoprene flux processing. Upper panel: determination of the FFT/CWT flux ratio; lower panel: application of flux divergence coefficients (derived in racetrack profiles) to scale fluxes from aircraft altitude to surface fluxes using aircraft altitude and PBL height.



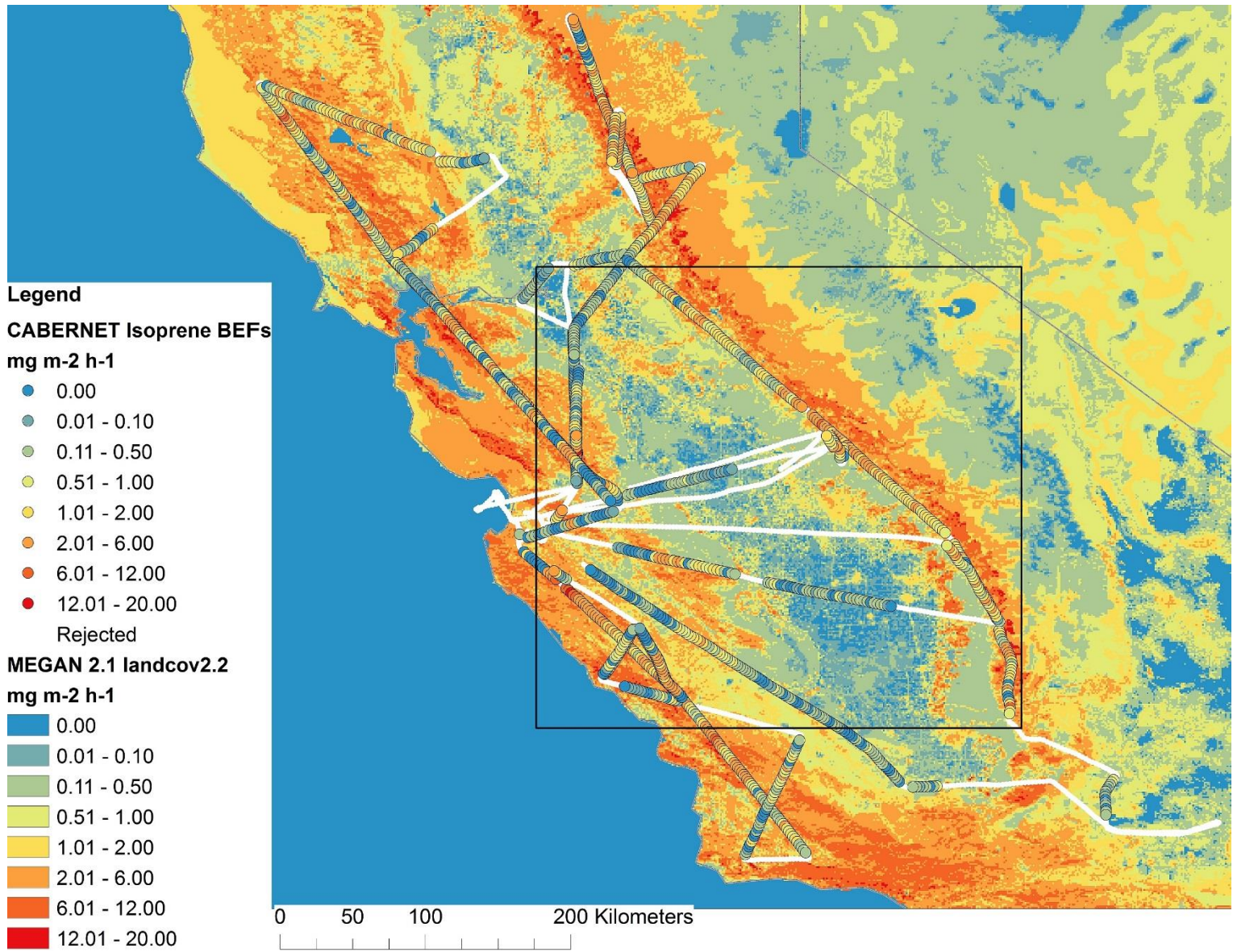
1  
2  
3  
4  
5  
6

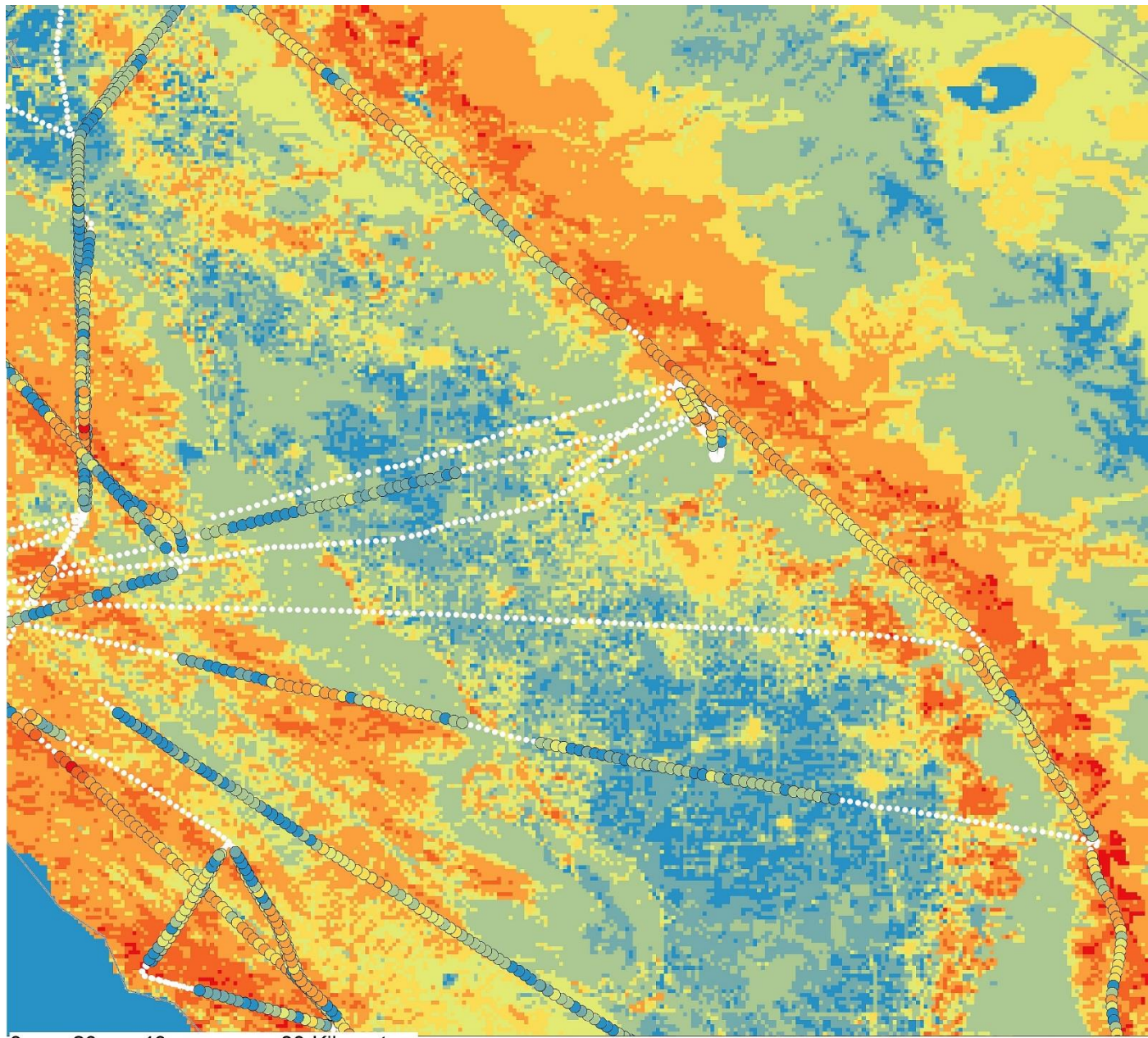
Figure 5. Spatial distributions of isoprene concentrations measured during CABERNET



1  
 2 Figure 6. Concentration gradients at Walnut Grove tower for a) m/z 69 (isoprene) and b) m/z  
 3 71 (dominated by MVK+MAC). When the aircraft was passing the tower both the tower's top  
 4 two inlet levels and the aircraft observed very low but non-zero concentrations of isoprene  
 5 and MVK+MAC. However, the tower data demonstrate that oxidation products of isoprene  
 6 routinely accumulate at night in the residual layer due to transport from the surrounding

- 1 foothills where emissions are high. The ground-airborne intercomparison is shown in
- 2 Supplementary information and Supplementary Fig. S3.





1



1 Figure 7. Comparison of airborne BEFs with MEGAN's landcover 2.2 for isoprene (airborne BEFs are subject to additional uncertainties  
2 introduced from T, and PAR and the algorithm's activity factor used in normalization). a) full extent with a rectangle denoting b) zoomed  
3 area.  
4